Research Article

JARO
Journal of the Association for Research in Otolaryngology

Check for updates

Super-enhancer Acquisition Drives FOXC2 Expression in Middle Ear Cholesteatoma

TOMOMI YAMAMOTO-FUKUDA[1,2] , NAOTARO AKIYAMA[2,3], AND HIROMI KOJIMA[1]

[1] *Department of Otorhinolaryngology, Jikei University School of Medicine, Tokyo, Japan*

[2] *Department of Histology and Cell Biology, Nagasaki University Graduate School of Biomedical Sciences, Nagasaki, Japan*

[3] *Department of Otorhinolaryngology, Toho University School of Medicine, Tokyo, Japan*

ABSTRACT

Distinct histone modifications regulate gene expression in certain diseases, but little is known about histone epigenetics in middle ear cholesteatoma. It is known that histone acetylation destabilizes the nucleosome and chromatin structure and induces gene activation. The association of histone acetylation with chronic inflammatory diseases has been indicated in recent studies. In this study, we examined the localization of variously modified histone H3 acetylation at lysine 9, 14, 18, 23, and 27 in paraffin-embedded sections of human middle ear cholesteatoma (cholesteatoma) tissues and the temporal bones of an animal model of cholesteatoma immunohistochemically. As a result, we found that there was a significant increase of the expression levels of H3K27ac both in human cholesteatoma tissues and the animal model. In genetics, super-enhancers are clusters of enhancers that drive the transcription of genes involved in cell identity. Super-enhancers were originally defined using the H3K27ac signal, and then we used H3K27ac chromatin immunoprecipitation followed by sequencing to map the active cis-regulatory landscape in human cholesteatoma. Based on the results, we identified increased H3K27ac signals as super-enhancers of the *FOXC2* loci, as well as increased protein of FOXC2 in cholesteatoma. Recent studies have indicated that menin-MLL inhibitor could suppress tumor growth through the control of histone H3 modification. In this study, we demonstrated that the expression of FOXC2 was inhibited by menin-MLL inhibitor in vivo. These findings indicate that FOXC2 expression under histone modifications promoted the pathogenesis of cholesteatoma and suggest that it may be a therapeutic target of cholesteatoma.

Keywords: FOXC2, Epigenetics, H3K27ac, Menin-MLL inhibitor, Middle ear cholesteatoma

INTRODUCTION

Epigenetic parameters such as DNA methylation and histone modifications play pivotal roles in disease, and histone modification is one of the major epigenetic parameters. Generally, acetylation of histones results in relaxed chromatin and transcriptional activation, whereas deacetylation of histone is associated with compacted chromatin and transcriptional repression. In fact, histone acetylation is an epigenetic event that plays a key role in the transcription of pro-inflammatory genes in chronic inflammatory diseases (Ito et al. 2005). For this reason, histone acetylation is often associated with a more open-chromatin conformation, and chromatin immunoprecipitation followed by sequencing (ChIP-Seq) analyses have confirmed the distribution of histone acetylation at promoters, enhancers and super-enhancers (SEs), detecting the transcribed region of the active genes (Heintzman et al. 2007; Wang et al., 2008; Dawson and Kouzarides 2012). A portion of the enhancer folds together, from the wide regions on chromatin with a high level of H3K27ac, and extends about

Correspondence to: Tomomi Yamamoto-Fukuda · Department of Otorhinolaryngology · Jikei University School of Medicine · Tokyo, Japan. email: tomomiyf@jikei.ac.jp

10 kb and sometimes even longer, which are called SEs (Chapuy et al. 2013; Lovén et al. 2013; Hnisz et al. 2013; Li et al. 2019). Super-enhancers contain high transcription activity and control the expression of master genes in the cell (Chapuy et al. 2013; Lovén et al. 2013; Hnisz et al. 2013). In tumor cells, SEs are the potential critical regulatory elements on chromatin, often associated with activated oncogenes (Hnisz et al. 2013). Therefore, the genomic landscapes of SEs in different diseases should be illustrated and the molecular mechanisms regulating the activity of SEs need to be elucidated.

It is well-known that middle ear cholesteatoma (cholesteatoma) is characterized by the presence of a keratinizing epithelium, which is believed to have hyper-proliferative properties (Kuo 2015). Our understanding of the molecular mechanism underlying the pathogenesis of cholesteatoma is limited, but an active proliferation of epithelial cells under inflammation creates irreversible change (Kuo 2015). Distinct histone modifications regulate gene expression in chronic inflammatory diseases, but little is known about this in cholesteatoma. In our previous study, we showed that stromal fibroblast growth factor 7 (FGF7)/keratinocyte growth factor (KGF) played an important role in human cholesteatoma formation, as characterized by the hyper-proliferation of epithelial cells (Tanaka et al. 1999; Yamamoto-Fukuda et al. 2003). In addition, the electrophoretic transfection of KGF gene-expressed vector induced cholesteatoma formation in vivo (Yamamoto-Fukuda et al. 2015). On the other hand, FGF signaling is known to control changes in the epigenetic signature, the level of histone modifications including acetylation of H3K27 (H3K27ac) and methylation of H3K4, and DNA methylation in the mouse embryonic stem cells during differentiation (Ficz et al. 2013). Recently, Tambalo and colleagues (2020) indicated that upon FGF signaling, activator protein 1 (AP1) recruits the histone acetylase p300 to some enhancers, which in turn promotes the H3K27ac associated with increased chromatin accessibility and enhancer activation in the developing ear. Based on the results, they showed that homeobox and winged-helix/forkhead proteins (Fox family) are possible cooperators with FGF-induced ear enhancers. H3K27ac as an important enhancer mark that distinguishes between active and poised enhancer elements (Creyghton et al. 2010). This mark can be deposited by p300 (Tie et al. 2009) and is associated with active promoters in mammalian cells (Wang et al. 2008). Indeed, the histone acetyl transferase (HAT) p300 especially increases levels of H3K27ac (Raisner et al. 2018). Physical interaction of AP1 and p300 has been shown in other research studies (Lee et al. 1996; Crish and Eckert 2008), and the inhibition of p300 prevents induction of some FGF response genes in cells (Tambalo et al. 2020).

These facts support the idea that KGF signaling under inflammation subsequently induces H3K27ac, which is required to activate some genes associated with the pathogenesis of cholesteatoma.

In this study, we initially examined the localization of variously modified histone H3 acetylation in paraffin-embedded sections of human cholesteatoma and normal skin (skin) tissues immunohistochemically, focusing on H3K9ac, H3K14ac, H3K18ac, H3K23ac, and H3K27ac. Increased levels of H3K27ac were observed in human cholesteatoma specimens. We then investigated H3K27ac ChIP-seq to map the active cis-regulatory landscape in human cholesteatoma. Based on the results, increased H3K27ac at the *FOXC2* gene locus—one among the Fox families—was observed in the cholesteatoma specimens and FOXC2 protein expression was confirmed in the human cholesteatoma tissues immunohistochemically. To investigate chromatin changes and FOXC2 expression patterns in the response to KGF signaling, we used an animal model of cholesteatoma that transfected the KGF-expression vector through the external auditory canal. The results showed an increasing level of H3K27ac and FOXC2 expression was observed in vivo. And moreover, we showed that H3K27ac inhibitor decreased FOXC2 expression in primary middle ear epithelial cells in vitro. According to the results from the human specimens, primary cells and the animal model, we postulated that transcription of *FOXC2* may be induced by H3K27ac generated through KGF signaling.

Menin is a highly specific binding partner of mixed-lineage leukemia 1 (MLL1), a histone methyltransferase that catalyzes H3K4me3 (Schuettengruber et al. 2007) and is required for the recruitment of the MLL1 complex to the target genes (Milne et al. 2005). The use of a menin-MLL1 inhibitor, MI503, in experiments has resulted in inhibition of the growth of tumors under a reduction in trimethylation of H3K4 histone modification (Malik et al. 2015). Interestingly, recent studies have demonstrated that menin, H3K4me3 and H3K27ac consists of looped enhancers and controls target gene expression (Dreijerink et al. 2017). It is known that looped enhancers are in direct physical contact with target promoters via chromatin looping and control gene activation and repression (Lee et al. 2015). Therefore, H3K4me3 and H3K27ac, which are contained looped enhancers, can control the same gene activation and repression (Dreijerink et al. 2017). In this study, we used MI503 to reduce the acetylation of H3K27 in the animal model to analyze the effects of H3K27ac against the transcription of *FOXC2*. Combined with the results from an inhibitor for the acetylation of H3K27, our objective was to demonstrate that histone modification on the cholesteatoma tissues might induce growth of cholesteatoma through the activation of FOXC2 expression.

MATERIALS AND METHODS

Subjects

Male ICR mice ($n = 7$, 8 weeks old, 33–37 g body weight) with normal ears were used in this study. All experiments were conducted according to the principles and procedures outlined in the guidelines for animal experimentation of Nagasaki University with the approval of the Institutional Animal Care and Use Committee (Nos. 1209241015-2 and 1404011269). Male BALB/c mice ($n = 12$, 6 weeks, 30–35 g, $n = 5$, 3 weeks, 15–20 g) with a normal tympanic membrane (TM) were used in this study. Animal care and experimental procedures were performed in accordance with the Guidelines for Animal Experimentation of Jikei University with approval guidelines (No. 2015-139C4).

Specimens from 35 ears with middle ear cholesteatoma, confirmed by histopathologic examination, were obtained from 22 men and 13 women (average age 46 years; range 2–85 years). For the analysis of FOXC2 expression, specimens from 25 ears with middle ear cholesteatoma, confirmed by histopathologic examination, were obtained from 21 men and four women (average age 39 years; range 10–69 years). All of the patients were treated surgically at the Department of Otorhinolaryngology, Jikei University Hospital, between May 2016 and December 2019. The cholesteatoma tissues were harvested from the patients during surgery. In 30 of the ears of the study subjects with cholesteatoma (17 males and 13 females; average age 53 years; range 9–80 years), a small piece of skin was harvested during surgery. For the analysis of FOXC2 expression, in 12 of the ears of the study subjects with cholesteatoma (10 males and 2 females; average age 54 years; range 29–72 years), a small piece of skin was harvested during surgery. This study protocol was approved by the Human Ethics Review Committee of Jikei University School of Medicine, and signed informed consent was obtained from all the patients or their guardians for this study (Approval Number: 27-344 8229).

Experimental Design

Animal Model of Middle Ear Cholesteatoma

Flag-human (h)KGF DNA plasmid driven by a CMV14 promoter (0.5 µg/ml) (KGF gene-transfected) or a null-plasmid driven by a CMV14 promoter (0.5 µg/ml) (vector alone-transfected) was transfected into the ICR mouse or BALB/c mouse ears using a Nepa21 Electroporator (Nepa Gene Co., Chiba, Japan), according to the protocol from a previous paper (Yamamoto-Fukuda et al. 2015). After the mice were anesthetized, each vector was injected into the cells of the external ear canal skin and TM. The hKGF cDNA expression vector was successfully transfected, and KGF protein was expressed 4 days after vector transfection, the same results as described previously both in the ICR mouse or BALB/c mouse ears (Yamamoto-Fukuda et al. 2015) (data not shown). KGF-expression vector was transfected five times every fourth day into the epithelial lesion of the ear of a prepared in vivo model (Yamamoto-Fukuda et al. 2015). The animals were euthanized using an intraperitoneal injection of 200 mg/kg pentobarbital. Their ear tissues were removed at day 4 and day 23 after vector transfection, fixed with 4% paraformaldehyde (PFA) in a phosphate-buffered saline (PBS) at 4 °C overnight, decalcified by 10% ethylenediaminetetraacetic acid at 4 °C for 7 days (Yamamoto-Fukuda et al. 2000) and then embedded in paraffin in the standard manner. The sections (5 µm thick) were prepared, and some were stained with hematoxylin and eosin (H&E) for histologic examination as previously described (Akiyama et al. 2014).

Administration of H3K27ac Inhibitor and Menin-MLL Inhibitor In vitro

Middle ear epithelial cells for the inhibition analysis of H3K27ac were prepared from male BALB/c mice (10 ears, 3 weeks) by the primary explant culture described previously (Yamamoto-fukuda et al. 2020). The cells were subcultured up to the third passage. The cells were plated on six-well plates at a sub-confluent concentration (60%) and incubated at 37 °C until they attached to the plating surface (Bowers et al. 2010). The same as for the vivo model, we administrated KGF protein to the cells for the middle ear cholesteatoma model in vitro. To study the H3K27ac signaling pathways, inhibitors were added before KGF protein was applied. The medium was replaced with low-glucose (1000 mg/l) Dulbecco's modified Eagle's medium containing 0.1% FBS (DMEM/0.1% FBS) 6 h before the cells were treated with inhibitors. The cells were treated with H3K27ac inhibitor (50 µM C646 in 2% DMSO in PBS [Li et al. 2019]) for 12 h, with menin-MLL inhibitor (0.5 µM MI503 in dimethyl sulfoxide (DMSO) in PBS (Borkin et al. 2015)) for 7 days or with 2% DMSO in PBS ($n = 4$ each). The medium was changed at day 4. Subsequently, recombinant human (rh) KGF/FGF7 (10 ng/ml (Braun et al. 2006)) or PBS was added, and the cells were incubated overnight.

Administration of Menin-MLL Inhibitor In vivo

Twelve male BALB/c mice (6 weeks) were used in the inhibition experiment. After confirming hKGF expression-vector transfection in the mouse ears, as had been done previously, 30 µl menin-MLL inhibitor (500 µM or 50 µM MI503 in 2% DMSO in PBS or 2% DMSO in PBS, $n = 4$ each) was administered in the ear skin region by eardrops for three consecutive days (day 1 to day 3) as described previously (Yamamoto-Fukuda et al. 2014). In accordance with the results of our previous study, we decided to

use the concentration of MI503 (Yamamoto-Fukuda et al. 2021). For the histopathological analysis, the ear tissues were removed at day 4 and paraffin sections of the ear tissues were prepared as described above.

REAGENTS

Chemicals and Biochemicals

The MI503 and C646 were purchased from Selleck Chemicals (Houston, TX). The rhKGF/FGF7 protein was purchased from Novus Biologicals USA (Centennial, CO). The protein/phosphatase inhibitor and skim milk were purchased from Cell Signaling Technology (Danvers, MA). The PFA was purchased from Merck (Darmstadt, Germany), and the 3 3′-diaminobenzidine 4HCl (DAB), Tween 20, and EDTA were purchased from Dojin Chemical Co. (Kumamoto, Japan). The 2×Laemmli's buffer was purchased from Bio-Rad (Hercules, CA), the polyvinylidene difluoride membranes were purchased from Immobilon-P, Millipore (Bedford, MA), and the ECL system was purchased from ECL Prime, GE Healthcare (Chicago, IL). The DMSO, 3-aminopropyltriethoxysilane, Tween20, bovine serum albumin (BSA, essentially fatty acid- and globulin-free), and 2-mercaptoethanol were purchased from Sigma Chemical Co. (St. Louis, MO, USA). The polyacrylamide gel and the permount were purchased from Thermo Fisher Scientific (Hudson, NH, USA). The 4,6′-diamidino-2-phenylindole dihydrochloride (DAPI) was purchased from Dako (Glostrup, Denmark). All other reagents used in this study were purchased from Wako Pure Chemicals (Osaka, Japan) and were of analytical grade.

Antibodies

The primary antibodies used in this study were anti-FOXC2 (mouse monoclonal, Sigma-Aldrich #WH0002303M2, 1:200 for the immunohistochemistry or 1:500 for the western blot analysis). Acetylation of histone H3 was detected by anti-H3K9ac (rabbit polyclonal, Cell Signaling Technology, Beverly, MA, USA #9671, 1:50), anti-H3K14ac (rabbit polyclonal, EPIGENTEK, Farmingdale, NY, USA #A-4023-025, 1:100), anti-H3K18ac (rabbit polyclonal, Cell Signaling Technology #9675, 1:100), anti-H3K23ac (rabbit polyclonal, Cell Signaling Technology #9674, 1:25), anti-H3K27ac (rabbit polyclonal, Abcam, Cambridge, UK, #ab45173, 1:100 for the immunohistochemistry or 1:5000 for the western blot analysis), and anti-β-actin (rabbit monoclonal, Cell Signaling Technology, #4970S, 1:1000), respectively. The secondary antibodies used in this study were Horseradish peroxidase (HRP)-conjugated goat anti-mouse IgG F(ab)' (Cell Signaling Technology, #7076, 1:10,000), HRP-conjugated goat anti-rabbit IgG F(ab)' (Cell Signaling Technology, #7074, 1:10,000), HRP-conjugated goat anti-mouse IgG F(ab)' (Abcam, #ab6789, 1:500), HRP-conjugated goat anti-rabbit IgG F(ab)' (Abcam, #ab6721, 1:500), Alexa Fluor 555-goat anti-mouse IgG (Thermo Fisher Scientific #A32727, 1:500), and Alexa Fluor 555-goat anti-rabbit IgG (Thermo Fisher Scientific #A 32,732, 1:500). The normal goat IgG was from Sigma Chemical Co. The normal mouse and rabbit IgG were from Dako. Detailed information about the antibodies is shown in Table 1.

Plasmids

The hKGF cDNA for the cording region was kindly provided by Dr. Jeffrey Rubin from the National Cancer Institute (Bethesda, MD). The 3X FLAG hKGF vector (Matsumoto et al. 2009) was constructed by inserting the cDNA to p3xFLAG–CMV14 vector (Sigma Chemical Co.).

Specific Methods

ChIP-seq

We outsourced H3K27ac ChIP-seq analyses to Active Motif, and a SE analysis was performed as previously described (Vijayakrishnan et al. 2019). For the H3K27ac

TABLE 1

List of primary antibodies for immunohistochemistry

Antibodies	Clone	Reactivity	Company	Cat no.	Dilution or concentration
Rabbit polyclonal anti-H3K9ac	NA	Mouse, rat, human, monkey, zebrafish	Cell Signaling	9671	1:50
Rabbit polyclonal anti-H3K14ac	NA	Mouse, human	EPIGENTEK	A-4023-025	1:100
Rabbit polyclonal anti-H3K18	NA	Mouse, rat, human	Cell Signaling	9675	1:100
Rabbit polyclonal anti-H3K23ac	NA	NA	Cell Signaling	9674	1:25
Rabbit monoclonal anti-H3K27ac	EP865Y	Mouse, rat, human	Abcam	ab45173	1:100
Mouse monoclonal anti-FOXC2	2H3	Mouse, rat, human	Sigma	WH0002303M2	1:200

ChIP-seq and SE analysis, frozen tissue (human cholesteatoma tissue and skin tissues from the external ear canal (200 mg each) were sent to Active Motif for ChIP and library preparation. The sample was divided into an aliquot for ChIP using an antibody to H3K27ac (Active Motif) and an input control. MACS or SICER peaks generated for the standard ChIP-seq analysis were used as "constituent enhancer" input to R. Young's SE software ROSE and the default settings for the Stitching Distance (12.5 kb) and transcription start site (TSS) Exclusion Zone (0 bp—no promoter exclusion) were used as described previously (Whyte et al. 2013; Lovén et al. 2013).

Immunohistochemistry

For the detection of H3K9ac, H3K14ac, H3K18ac, H3K23ac, H3K27ac, and FOXC2, an enzyme or fluorescence immunohistochemistry was performed on the paraffin sections, as described previously (Yamamoto-Fukuda et al. 2014, 2015; Akiyama et al. 2014; Song et al. 2011). The sections were autoclaved in a 0.01 M citrate buffer (pH 6.0) at 95 °C for 15 min to retrieve the antigen. For the enzyme immunohistochemistry after the inactivation of endogenous peroxidase with 0.3% H_2O_2 in methanol for 15 min, the slides were preincubated with 500 μg/ml normal goat IgG in 1% bovine serum albumin (BSA) in PBS for 1 h to block a nonspecific reaction. The sections were then reacted overnight with the first antibody in 1% BSA in PBS. After reaction with the HRP-conjugated second antibody, the sites of HRP were visualized with DAB and H_2O_2, or in the presence of nickel and cobalt ions. For the fluorescence immunohistochemistry after immersion with the first antibody, the sections were incubated with the second antibody (Alexa Fluor 555-goat anti-mouse IgG or Alexa Fluor 555-goat anti-rabbit IgG) for 1 h. After washing three times with 0.05% Tween 20 in PBS, the sections were counterstained with DAPI. For every experimental run, negative control samples were prepared by reacting the sections with normal mouse IgG or normal rabbit IgG instead of the specific first antibody.

Western Blot Analysis

For the detection of H3K27ac, FOXC2, and β-actin, a western blot analysis was performed as described previously (Yamamoto-Fukuda et al. 2020). The cells (5.0×10^5 cells) were washed with PBS and lysed using buffer (2× Laemmli's buffer and 2-mercaptoethanol, protein/phosphatase inhibitor). Cell lysates were centrifuged twice at 18,000 rpm for 5 min at 4 °C. Proteins were then separated by polyacrylamide gel and transferred electrophoretically onto polyvinylidene difluoride membranes. The membranes were blocked with 5% skim milk in 0.1% Tween 20 in tris buffered saline for 1 h at room temperature (RT) and immersed with first antibodies diluted in a 2.5% blocking buffer at 4 °C overnight. The antibody-antigen complexes were detected using HRP goat anti-mouse IgG or rabbit IgG (1:10,000 dilution) for 1 h at RT. The signals were visualized by the ECL system and photographs were taken using a chemiluminescence imager (LAS 4000; GE Healthcare). A quantification data analysis was performed using ImageJ software ver. 15.1 (NIH, https://imagej.nih.gov/ij/) (Schneider et al. 2012), and the signal strength was sdetermined using the intensity of the band divided by the β-actin band intensity, establishing β-actin protein levels as a loading control.

Microscopy, Image Analysis, and Cell Count

Images of the H&E staining and enzyme-immunostaining were captured using an Axio Cam camera and AxioVision software (Carl Zeiss, Jena, Germany) under light microscopy. Fluorescent images were obtained using fluorescence confocal laser scanning microscopy (LSM 880, Carl Zeiss). For the quantitative analysis, the enzyme-immunohistochemistry results were graded as positive or negative as compared with the negative control, and the number of cell nuclei was counted at more than 1000 nuclei in three equal epithelial regions at × 400 magnification. Per specimen of immunofluorostaining, three 10,000 μm^2 areas (100 × 100 μm squares) for the equal epithelial regions were assumed with confocal laser scanning microscopy (LSM 880) and Zeiss acquisition analysis software (Zen Black), and the number of positive cell nuclei was counted. DAPI labeling was used to obtain the total cell number. The labeling index (LI) [mean ± SD] represented the percentage of positive cell nuclei per the total number of counted nuclei. The thickness of the epithelium was measured at four locations (central and at each extreme) using NIH Image/ImageJ software as described previously (ver. 1.46r) (Schneider et al. 2012).

Statistical Analysis

All data were expressed as mean ± SD. Differences between the groups were examined for statistical significance using the one-way analysis of variance (ANOVA) test followed by an unpaired t test or Tukey's post hoc test for normally distributed data. A P value of less than 0.05 denoted the presence of a statistically significant difference. All analyses

were performed using a statistical software package (JMP version 13; SAS Institute Japan, Tokyo, Japan). Precise values for P are given in the results for all significant differences, as stipulated in the guidelines for JARO publications.

RESULTS

Acetylation Levels of Histone H3 at Lysine 9, 14, 18, 23, and 27 in Human Middle Ear Cholesteatoma and Normal Skin Tissue

According to the results of the immunohistochemistry of anti-H3K9ac, anti- H3K14ac, and anti- H3K18ac, the localization and frequency of positive cells are almost the same in the sections of cholesteatoma and skin. H3K9ac-positive cells were scarcely detected but many H3K14ac-positive cells and H3K18ac-positive cells were detected in the keratinizing squamous epithelium and subepithelial region of the cholesteatoma tissue and skin (Fig. 1a). H3K9ac LI ($n = 35$, 40.74 ± 23.0%) and H3K14ac LI ($n = 35$, 57.70 ± 23.0%) in the cholesteatoma were almost the same as that of skin tissue ($n = 30$ for each, H3K9ac LI: 39.65 ± 20.2% and H3K14ac LI: 59.90 ± 21.6%) (Fig. 1b). However, H3K18ac LI in cholesteatoma ($n = 35$, 63.47 ± 18.8%) was significantly higher than that of skin ($n = 30$, 47.13 ± 26.8%) (one-way ANOVA $F(1, 63) = 8.27$, $p < 0.01$ with an unpaired t test) (Fig. 1b). On the other hand, a large number of H3K23ac-positive cells and H3K27ac-positive cells were detected in the basal and upper layers of the thickened wall of the cholesteatoma matrix and the subepithelial region but scarcely detected in the section of skin (Fig. 1a). H3K23ac LI in cholesteatoma ($n = 35$, 63.45 ± 21.0%) was significantly higher than that of skin ($n = 30$, 35.28 ± 21.5%) (one-way ANOVA $F(1, 63) = 28.46$, $p < 0.0001$ with an unpaired t test) (Fig. 1b). H3K27ac LI in cholesteatoma ($n = 35$, 61.69 ± 22.2%) was significantly higher than that of skin ($n = 30$, 29.57 ± 13.3%) (one-way ANOVA $F(1, 63) = 48.08$, $p < 0.0001$ with an unpaired t test) (Fig. 1b). All of the results of the statistical analysis are listed in Table 2.

H3K27ac ChIP-seq Data in the Skin and Cholesteatoma

H3K27ac is an epigenetic mark that is frequently present in promoters or enhancers, which also separates active enhancers from poised enhancers. To examine whether cholesteatoma differential gene expression may be functionally linked with differential H3K27 acetylation, we performed ChIP-seq studies to profile global differential gene expression and differential H3K27 acetylation, for both the human cholesteatoma and skin specimens. As shown in Fig. 2a, the number of active region profiles marked by H3K27ac in cholesteatoma ($n = 38,264$) was

more than that of the skin ($n = 25,295$) specimens. The genomic features had some differences between the skin and cholesteatoma (skin vs. cholesteatoma: 11,607 vs. 18,054 in introns, 3660 vs. 3339 in exons, 687 vs. 684 in the 3′-UTR, 3025 vs. 2496 in the 5′-UTR, 3496 vs. 3381 in 1 kb upstream, and 5756 vs. 9832 in intergenic regions), and the genomic distribution of cholesteatoma versus that of skin is schematically illustrated in Fig. 2b.

The ChIP-seq analysis revealed that a genome-wide increase of H3K27ac with regional gains in H3K27ac levels was detected in the cholesteatoma specimens as compared with that of the skin specimens (Fig. 1c, slope value > 1, Pearson's correlation coefficient = 0.941, slope 2.0216.) Heatmaps and plots of H3K27ac ChIP-seq data revealed that global H3K27ac signals in the active regions, gene bodies and promoter regions (TSS) were increased, with a two-fold increase in the cholesteatoma specimens against those of skin (Fig. 2c). In the cholesteatoma specimens, increased of H3K27ac was seen in terms of the forkhead box protein C2 (*FOXC2*), which belongs to the Fox family; *PRKCH*, a family of serine- and threonine-specific protein kinases; and *PPP1R16B*, which is a regulator of protein phosphatase 1 (Fig. 2d).

Super-enhancers are large clusters of enhancers that regulate the activity of key genes during development and disease pathogenesis (Lovén et al. 2013; Whyte et al. 2013). H3K27ac is one of the best-characterized epigenetic marks for mapping genome-wide SE structures (Creyghton et al. 2010; Raisner et al. 2018). To test whether the pathogenesis of cholesteatoma may alter SEs to modulate its target gene activities, we used the ROSE algorithm to map SEs in both skin and cholesteatoma. Higher signals ranked by H3K27ac were designated as SEs (Fig. 2f). A total of 750 SEs was identified in skin specimens. As compared to the results for the skin, the total number of SEs increased to 942 SEs in the cholesteatoma specimens, respectively (Fig. 2f). Among the detected genes in ChIP-seq, which were shown in Fig. 2e, an increased H3K27ac signal of the SE associated with *FOXC2* was observed in the cholesteatoma specimens compared with the results for the skin specimens (Fig. 2G).

Analysis of FOXC2-Expression in Human Tissues

To confirm that the protein expression of FOXC2 played a role in the pathogenesis of cholesteatoma, we analyzed the expression of FOXC2 by immunohistochemistry in the cholesteatoma and skin tissues. As shown in Fig. 3a, FOXC2 protein was detected in the basal and upper layers of the epithelium and subepithelial region in the cholesteatoma. In contrast, a small number of FOXC2-positive cells were found, mainly in the basal layer of the epithelium but rarely detected in the subepithelial region in the skin (Fig. 3a). No staining was detected with normal mouse IgG instead of with the first antibody
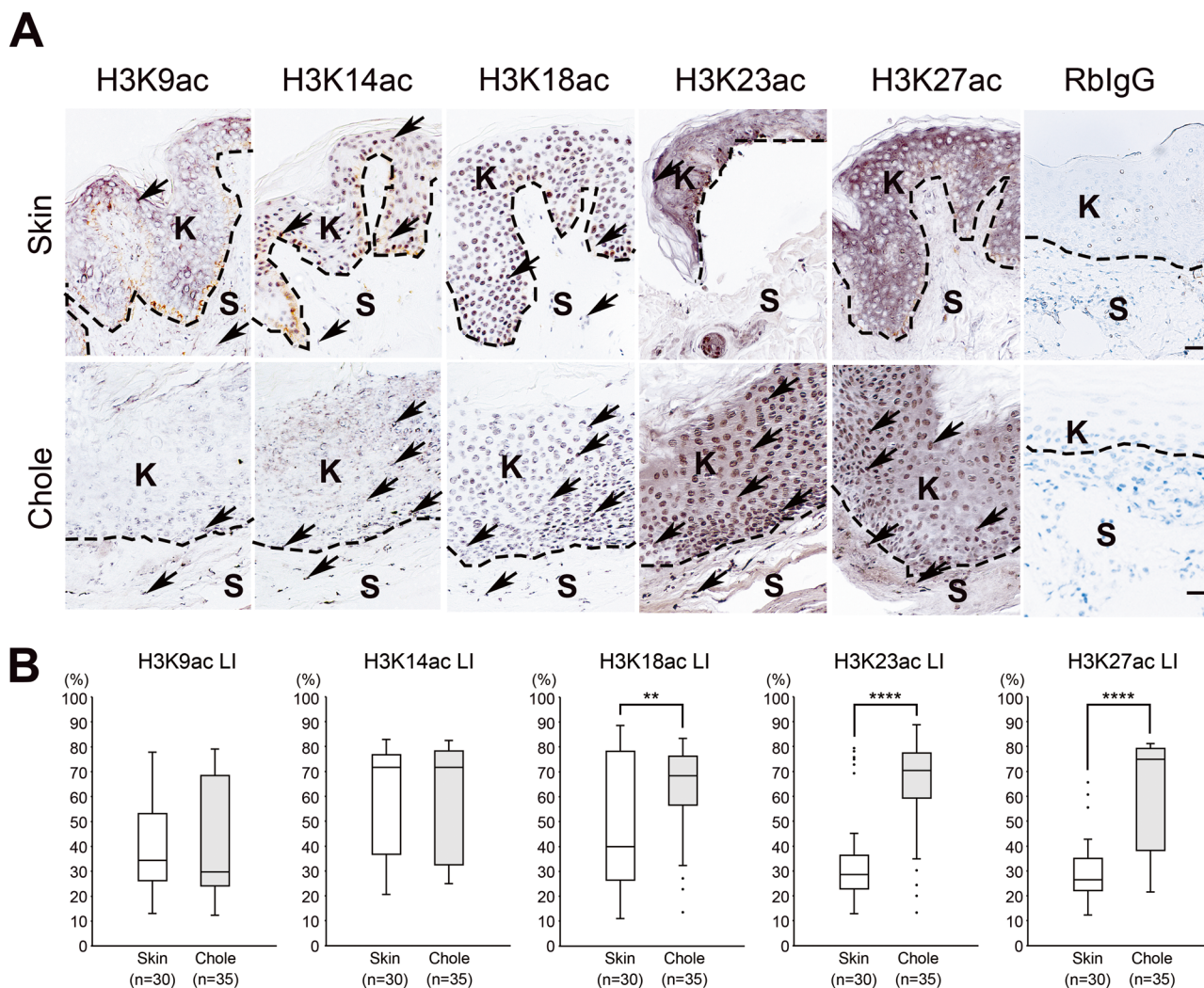
FIG. 1 a Immunohistochemical detection of acetylated histone H3 at lysine 9, 14, 18, 23, and 27 in paraffin-embedded human normal skin (skin, upper panels) and middle ear cholesteatoma (chole, lower panels) tissues. Some H3K9ac-positive cells were detected in keratinizing squamous epithelium and subepithelial region in the sections of skin and chole. Many H3K14ac-positive cells and H3K18ac-positive cells were detected in keratinizing squamous epithelium in the sections of skin and chole. H3K23ac-positive cells and H3K27ac-positive cells were detected in keratinizing squamous epithelium and subepithelial region in the sections of chole, but scarcely detected in the section of skin. Normal rabbit IgG (Rb IgG) was used instead of first antibody as a negative control. Arrows indicate positive cells. Dashed lines indicate the basement membrane. K indicates keratinizing squamous epithelium. S indicates the subepithelial region. Scale bars, 20 μm. b Box plot showing the labeling index (LI) of acetylated histone H3 at lysine 9, 14, 18, 23, and 27 positive cells in skin (white boxes, $n = 30$ for each) vs. chole (gray boxes, $n = 35$ for each). One-way ANOVA with an unpaired t-test were used to compare each LI of skin versus chole; H3K18ac LI: $F_{(1, 63)} = 8.27$, **, $p < 0.01$; H3K23ac LI: $F_{(1, 63)} = 28.46$, ****, $p < 0.0001$: H3K27ac LI: $F_{(1, 63)} = 48.08$, ****, $p < 0.0001$

(Fig. 3a). High levels of FOXC2 LI were observed in the epithelium of the cholesteatoma ($n = 25$, $34.43 \pm 8.8\%$) versus that of the skin ($n = 12$, compared to $3.64 \pm 2.3\%$) (one-way ANOVA $F_{(1, 35)} = 139.17$, $p < 0.0001$ with a Student t test) (Fig. 3b, Table 2). In addition, FOXC2 LI in the subepithelial region of cholesteatoma specimens ($n = 25$, $34.83 \pm 9.9\%$) was significantly higher than that in the skin specimens ($n = 12$, $4.19 \pm 2.3\%$) (one-way ANOVA $F_{(1, 35)} = 139.17$, $p < 0.0001$ with an unpaired t test) (Fig. 3b, Table 2).

Acetylation Level of Histone H3 at Lysine 9, 14, 18, 23, and 27 in KGF cDNA-Transfected Mouse Ear Skin

The FLAG-hKGF expression vector or vector alone was transfected into the mouse ear, according to the protocol of a previous paper (Yamamoto-Fukuda et al. 2015) (Fig. 4a). The FLAG-hKGF expression vector was successfully transfected in vivo and induced KGF expression

TABLE 2

The results of LI of H3K9ac, 14ac, 18ac, 23ac, and 27ac-positive cells, and FOXC2-positive cells in human specimens and vector transfected-mouse ears

	H3K9ac	H3K14ac	H3K18ac	H3K23ac	H3K27ac	FOXC2
Human						
Cholesteatoma	40.74 ± 23.0 (n = 35)	57.70 ± 23.0 (n = 35)	63.47 ± 18.8 (n = 35)**	63.45 ± 21.0 (n = 35)****	61.69 ± 22.2 (n = 35)****	34.83 ± 9.9 (n = 25)****
Skin	39.65 ± 20.2 (n = 30)	59.90 ± 21.6 (n = 30)	47.13 ± 26.8 (n = 30)	35.28 ± 21.5 (n = 30)	29.57 ± 13.3 (n = 30)	4.19 ± 2.3 (n = 12)
Mouse day 4						
KGF gene	28.40 ± 3.1 (n = 3)	21.72 ± 4.7 (n = 3)	77.04 ± 4.8 (n = 3)**	52.78 ± 11.1 (n = 3)	35.53 ± 2.5 (n = 3)****	
Vector alone	28.07 ± 3.2 (n = 3)	22.08 ± 4.5 (n = 3)	35.93 ± 6.8 (n = 3)	52.55 ± 3.9 (n = 3)	9.83 ± 0.7 (n = 3)	
Mouse day 23						
KGF gene/ Chole					55.54 ± 7.6 (n = 4)****	49.07 ± 7.1 (n = 4)****
Vector alone					20.14 ± 6.4 (n = 4)	5.10 ± 2.1 (n = 4)

****$p < 0.0001$, ***$p < 0.001$, **$p < 0.01$

until day 4, the same as the results described previously (Yamamoto-Fukuda et al. 2015) (data not shown).

According to the results of the immunohistochemistry, a large number of H3K27ac-positive cells were detected in the basal and upper layers of the thickened epithelium and subepithelial region of the KGF gene-transfected ears at day 4, but were scarcely detected in the sections of the vector alone-transfected ears at day 4 (Fig. 4b). H3K27ac LI in the KGF gene-transfected ears (day 4, $n = 3$, 35.53 ± 2.5%) was significantly higher than that of the vector alone-transfected ears (day 4, $n = 3$, 9.83 ± 0.7%) (one-way ANOVA $F(1, 4)$ 293.74, $p < 0.0001$ with an unpaired t-test) (Fig. 4c). H3K18ac-positive cells were detected in the basal and upper layers of the epithelium and subepithelial region in sections of both the KGF gene-transfected ears and vector alone-transfected ears; however, the H3K18ac-positive rate of the KGF gene-transfected ears (day 4, $n = 3$, 77.04 ± 4.8%) was significantly higher than that of the vector alone-transfected ears (day 4, $n = 3$, 35.93 ± 6.8%) (one-way ANOVA $F(1, 4) = 72.23$, $p < 0.01$ with an unpaired t test) (Fig. 4c). On the other hand, the results of the immunohistochemistry of anti-H3K9ac, anti-H3K14ac and anti-H3K23ac, the localization and frequency of positive cells was almost same in the sections of both the KGF gene-transfected and vector alone-transfected ears. Some H3K9ac-positive and H3K14ac-positive cells and many H3K23ac-positive cells were detected in the epithelium and subepithelial regions of the KGF gene-transfected and vector alone-transfected ears (data not shown). H3K9ac LI (day 4, $n = 3$, 28.40 ± 3.1%), H3K14ac LI (day 4, $n = 3$, 21.72 ± 4.7%), and H3K23ac

LI (day 4, $n = 3$, 52.78 ± 11.1%) in the KGF gene-transfected ears were almost the same as that of the vector alone-transfected ears (day 4, $n = 3$ for each, H3K9ac LI 28.07 ± 3.2%, H3K14ac LI 22.08 ± 4.5%, and H3K23ac LI 52.55 ± 3.9%) (Fig. 4c).

Immunohistochemical Analysis of Acetylation of H3K27 and FOXC2 Expression in KGF-Induced Cholesteatoma In vivo

At day 23 after vector transfection, an immunohistochemical analysis for H3K27ac was performed to evaluate the effects of KGF gene transfection against the histone modification of epithelial cells of KGF-induced cholesteatoma (Fig. 4a). H&E staining revealed that the epithelial and intermediate layers of the pars flaccida (PF) of the TM of the KGF gene-transfected ears were thickened with debris and consistent cholesteatoma formation, the same results as described previously (Yamamoto-Fukuda et al. 2015) (Fig. 4d). In this thickened TM, the number of H3K27ac-positive cells had increased in the epithelial, intermediate and mucosal layers (Fig. 4e). In contrast, FOXC2-positive cells were observed mainly in the intermediate and mucosal layer of the PF in the KGF gene-transfected ears (Fig. 4e). Some of the epithelial cells of the PF were FOXC2-positive in the KGF gene-transfected ears (Fig. 4e). On the other hand, the TM of the vector-alone transfected ears appeared as normal, thin, squamous epithelium (Fig. 4d). In the control ears, H3K27ac-positive cells and FOXC2-positive cells were scarcely detected in the TM (Fig. 4e). H3K27ac LI in the KGF

gene-transfected ears at day 23 ($n = 4$, $55.54 \pm 7.6\%$) was significantly higher than that in the vector alone-transfected ears at Day 23 ($n = 4$, $20.14 \pm 6.4\%$; one-way ANOVA $F(1, 6) = 50.64$, $p < 0.001$ with an unpaired t-test) (Fig. 4f, Table 2). Higher FOXC2 LI was observed in the subepithelial region of the PF after KGF gene transfection, compared to the vector alone transfection ($n = 4$ for each, $49.07 \pm 7.1\%$ vs. $5.10 \pm 2.1\%$; one-way ANOVA $F(1, 6) = 142.34$, $p < 0.0001$ with an unpaired t test) (Fig. 4f, Table 2).

Inhibition of H3K27ac Repressed the Expression of FOXC2 In vitro

To examine the role of H3K27ac under KGF induction against the expression of FOXC2 in middle ear epithelial cells, we administered one reported inhibitor for H3K27ac, C646 (Li et al. 2019) in vitro. As expected, the level of acetylation of H3K27 was upregulated under KGF administration in the middle ear epithelial cells (KGF + versus KGF-, 2.30 versus 0.11) (Fig. 5a). H3K27ac inhibitor or a menin-MLL1 inhibitor administration (50 µM C646, 0.5 µM MI503, $n = 4$ for each) was performed before KGF protein administration in vitro. According to the results, the anti-H3K27ac polyclonal antibody detected H3K27ac protein in the control group, C646 group, and MI503 group (Fig. 5b), but the intensity of the bands of the C646 group and MI503 group was lower than that of the control group (C646, MI503 versus control, 0.10, 0.19 versus 2.37) (Fig. 5c). We found that the treatment of C646 or MI503 to the middle ear epithelial cells inhibited acetylation of H3K27, indicating that the drugs were functional (Fig. 5b, c). Anti-FOXC2 polyclonal antibody detected FOXC2 protein in the control group but slightly detected it in the C646 group and MI503 groups (Fig. 5b). The intensity of the bands of the C646 group and MI503 group was lower than that of the control group (C646, MI503 versus control, 0.01, 0.10 versus 0.27) (Fig. 5c). These data suggest that the acetylation of H3K27 controls expression of FOXC2 in middle ear epithelial cells.

Detection of FOXC2-Positive Cells of KGF-Transfected Mouse Ear Skin Tissue After Menin-MLL1 Inhibitor Treatment

To examine the effects of H3K27ac under KGF induction against the expression of FOXC2 in the ear tissues, a menin-MLL1 inhibitor administration (KGF with 50 µM MI503, KGF with 500 µM MI503, $n = 4$ for each) was performed after KGF gene transfection in vivo (Fig. 6a). As a vehicle, 2% DMSO in PBS was used instead of MI503 (KGF with PBS, $n = 4$). H&E staining of the mouse ear skin tissues revealed that KGF gene transfection with 2% DMSO in PBS induced a marked thickening of the epithelium, as compared to that for KGF gene

transfection with MI503-treated ear skin tissue (Fig. 6b). The thickness of the epithelium of KGF with 2% DMSO in PBS reached a maximum (86.89 ± 31.7 µm). On the other hand, the thickness of the epithelium of KGF with 50 µM MI503 (31.46 ± 10.1 µm) and of KGF with 500 µM MI503 (47.91 ± 18.6 µm) was significantly reduced (one-way ANOVA $F(2, 9) = 6.69$, $p = 0.0152$ and $p = 0.0783$, respectively, with Tukey's post hoc test) (Fig. 6c, Table 3). The number of H3K27ac-positive cells was dramatically lower in the subepithelial region, and almost no positive epithelial cells were found in the KGF gene-transfected ear skin tissue treated with 50 µM or 500 µM MI503 (Fig. 6d). However, intensely stained epithelial cells were detected in KGF gene-transfected ear skin tissue treated with 2% DMSO in PBS (Fig. 6d). H3K27ac LI of the MI503-treated ears (KGF with 50 µM MI503 $8.74 \pm 2.5\%$, KGF with 500 µM MI503 $8.25 \pm 1.2\%$) was significantly lower than that of the 2% DMSO in PBS-treated ears ($36.73 \pm 2.2\%$) (one-way ANOVA $F(2, 9) = 253.56$, $p < 0.0001$ with Tukey's post hoc test) (Fig. 6e, Table 3). As expected, acetylation of histone H3K27 induced under KGF expression was inhibited by the menin-MLL inhibitor MI503. According to the results of an immunohistochemical analysis of FOXC2, positive cells were detected in the subepithelial region of KGF with 2% DMSO in PBS (Fig. 6d). On the other hand, MI503 inhibits FOXC2 expression in the cells of the subepithelial region induced by KGF gene transfection (Fig. 6d). In contrast to the vehicle, FOXC2-positive cells were scarcely detected (Fig. 6d). At day 4 after KGF transfection, FOXC2 LI of the MI503-treated ears (50 µM MI503: $7.56 \pm 2.8\%$, 500 µM MI503: 8.29 ± 4.4) was significantly lower than that of the PBS-treated ears ($32.11 \pm 2.5\%$) (one-way ANOVA $F(2, 9) = 69.88$, $p < 0.0001$ with Tukey's post hoc test) (Fig. 6e, Table 3).

DISCUSSION

Induction of Acetylation of HistoneH3K27-Activated *FOXC2* Gene Transcription in Human Cholesteatoma Specimens

It is well known that cholesteatoma is characterized by the presence of a keratinizing epithelium with a subepithelial region that is believed to have hyper-proliferative properties under chronic inflammation (Sudhoff and Tos 2000). Our understanding of the molecular mechanism underlying the pathogenesis of cholesteatoma is limited, but an active proliferation of epithelial cells under stimulation of proinflammatory cytokine is thought to be irreversible (Chi et al. 2015). According to the results of recent studies that indicated the correlation between histone acetylation and inflammatory disease (Ito et al.
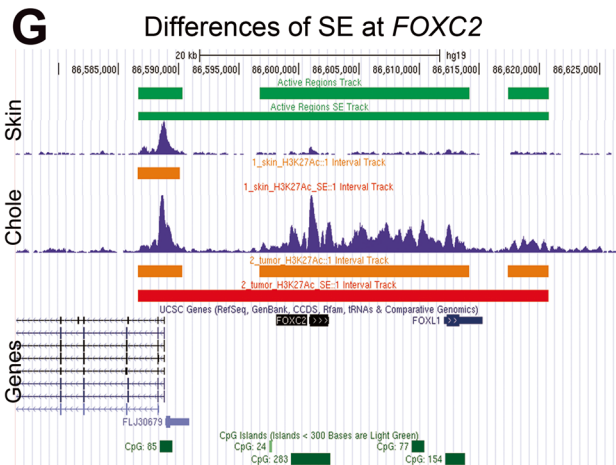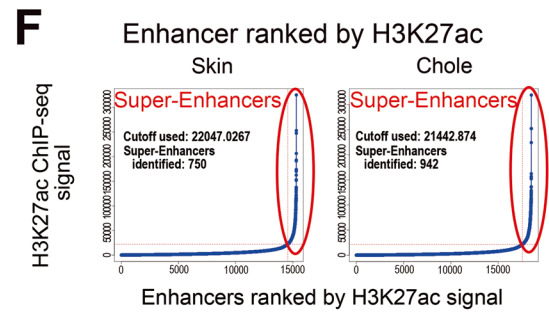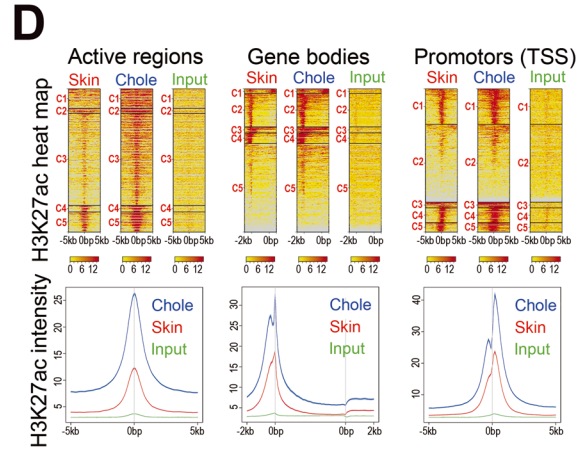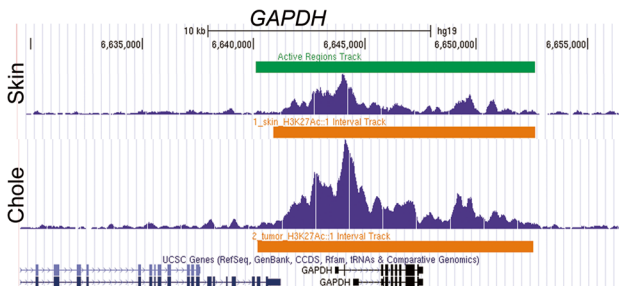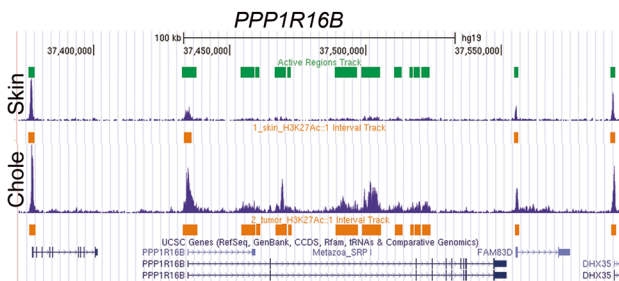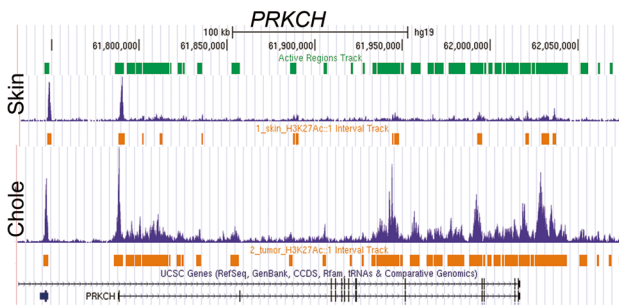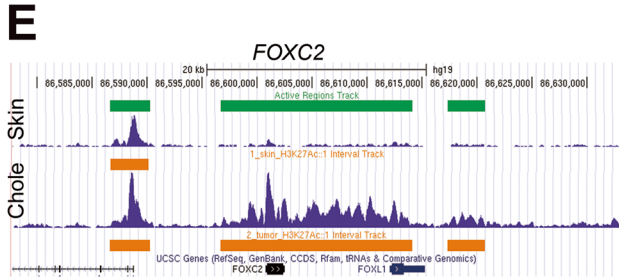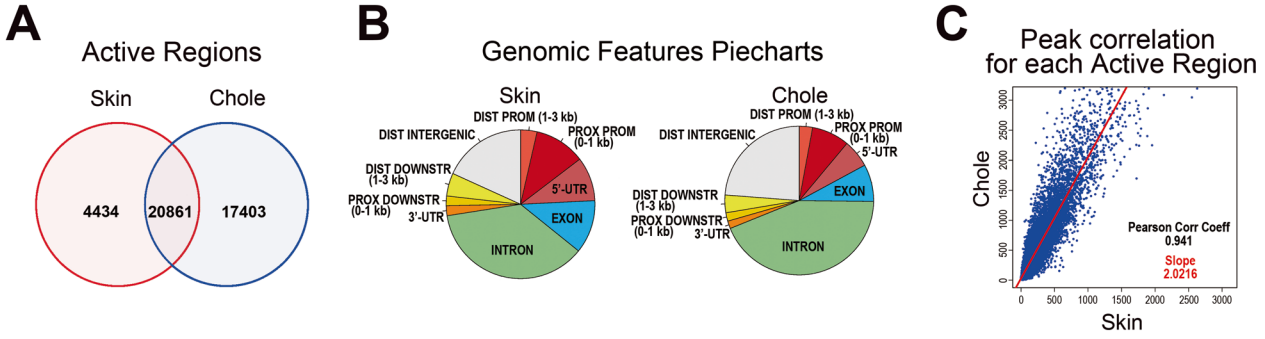
◄ **FIG. 2** H3K27ac ChIP-seq data in the normal skin (skin) and middle ear cholesteatoma (chole). **a** Venn diagram showing the number of active regions marked by H3K27ac in skin (25,295) and chole (38,264) specimens. Total number of Active region profiles marked by H3K27ac were increased in chole. **b** Genomic features pie charts of skin and chole. **c** The peak correlation for each active region between skin and chole. The progressive gain of H3K27ac was shown in chole specimens. *x/y* values are tag numbers in merged peak regions. Slope value > 1 indicates a gain of H3K27ac; Pearson's correlation coefficient = 0.941, slope 2.0216. **d** Heatmaps and plots of H3K27ac ChIP-seq data for active regions, gene bodies and promotors (TSS) of skin and chole specimens. **e** Visualization of H3K27ac ChIP-seq data in the UCSC genome browser. Screenshot of UCSC genome browser showing H3K27ac ChIP-seq results in the skin and chole specimens. The chole specimens increased H3K27ac at the *FOXC2* gene locus, *PRKCH* gene locus, and *PPP1R16B* gene locus. *FOXC2*: forkhead box protein C2; *PRKCH*: protein kinase C eta type, serine 11B; *PPP1R16B*: protein phosphatase 1 regulatory subunit 16B. **f** Enhancers in skin and chole specimens identified by the ROSE program were ranked and plotted by H3K27ac ChIP-seq signal. Each blue dot represents an enhancer, in which the one above the inflection point of the curve was defined as super-enhancers (SE) (red circle areas). **g** Visualization of gained SE at *Foxc2* locus by H3K27ac ChIP-seq data in the UCSC genome browser

2005), we focused on the acetylation level of histone H3 in cholesteatoma tissues.

As expected, in this study we clearly demonstrated that many H3K18ac-positive, H3K23ac-positive and H3K27ac-positive epithelial cells were detected in human cholesteatoma specimens (Fig. 1). Gene expression regulation may be co-determined by a combination of other histone modifications, including the acetylation of H3K9, H3K18 (Ernst et al. 2011; Zentner et al. 2011), and H3K27 that are linked with active enhancers and promoters (Djebali et al. 2012; Heintzman et al. 2007). Among these, we focused on H3K27ac mainly because it is one

of the best-characterized epigenetic marks associated with active enhancer and promoter regions (Creyghton et al. 2010; Calo and Wysocka 2013). The open chromatin regions marked by H3K27ac may be indicative of the frequent binding of transcription factors and large genomic regions, so-called SEs (Hnisz et al. 2013; Whyte et al. 2013). Super-enhancers contain high transcription activity and control the expression of cell identity genes (Hnisz et al. 2013; Whyte et al. 2013). As a next step, we moved onto investigating H3K27ac ChIP-seq.

In a previous study, we indicated that KGF enhanced epithelial cell proliferative activity and correlated to the recurrence of human cholesteatoma (Yamamoto-Fukuda et al. 2003). In addition, the repetitive electroporatic transfection of the KGF gene expression vector induced middle ear cholesteatoma formation in vivo (Yamamoto-Fukuda et al. 2015). In the recent study, the activation of *FOXD3*, one of the Fox families, was shown upon FGF signaling with acetylation of H3K27 during mouse ear development (Tambalo et al. 2020). Based upon these observations, we hypothesized that cholesteatoma formation might be induced by the expression of *FOXD3* with histone modification under KGF signaling. However, based on the results related to H3K27ac ChIP-seq, we found active changes in the *FOXC2* gene locus associated with the SEs and FOXC2 protein expression, another member of the Fox family, in the cholesteatoma specimens as compared to the skin specimens (Fig. 2, Fig. 3). FOXC2 has recently been reported to be involved in cancer progression and metastasis, and a high expression of FOXC2 is an independent prognostic factor in esophageal cancer, gastric cancer, and non-small-cell lung cancer (Nishida et al. 2011; Zhu et al. 2013; Jiang et al. 2012). In a recent study, Imayama and colleagues (2015) detected that the expression of FOXC2 was
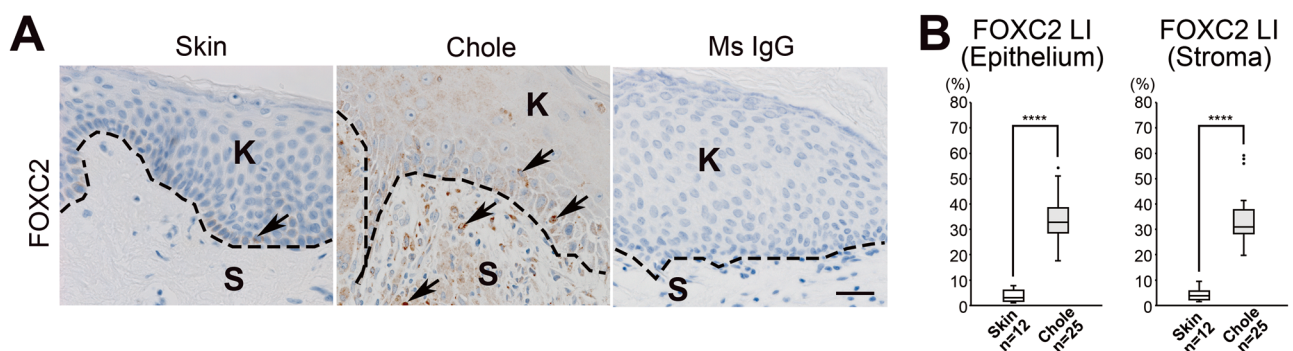
FIG. 3 Detection of FOXC2-expression in human middle ear cholesteatoma tissues and skin. **a** Immunohistochemical analysis using the anti-FOXC2 antibody in the sections of skin and chole. FOXC2-positive cells were detected in the basal layer of the epithelium of skin. In the section of chole many FOXC2-positive cells were shown in keratinizing squamous epithelium and subepithelial region. Normal mouse IgG (Ms IgG) was used instead of first antibody as a negative control. Arrows indicate positive cells. Dashed lines indicate the basement membrane. K indicates keratinizing squamous epithelium. S indicates the subepithelial region. Scale bar, 20 μm. **b** Box plot showing the labeling index (LI) of FOXC2-positive cells in the epithelium (epithelium) or subepithelial region (stroma) of skin (white boxes, $n = 12$) vs. chole (gray boxes, $n = 25$). One-way ANOVA with an unpaired *t* test were used to compare FOXC2 LI of skin versus chole; in epithelium: $F(1, 35) = 139.17$, ****, $p < 0.0001$; in stroma: $F(1, 35) = 110.50$, ****, $p < 0.0001$
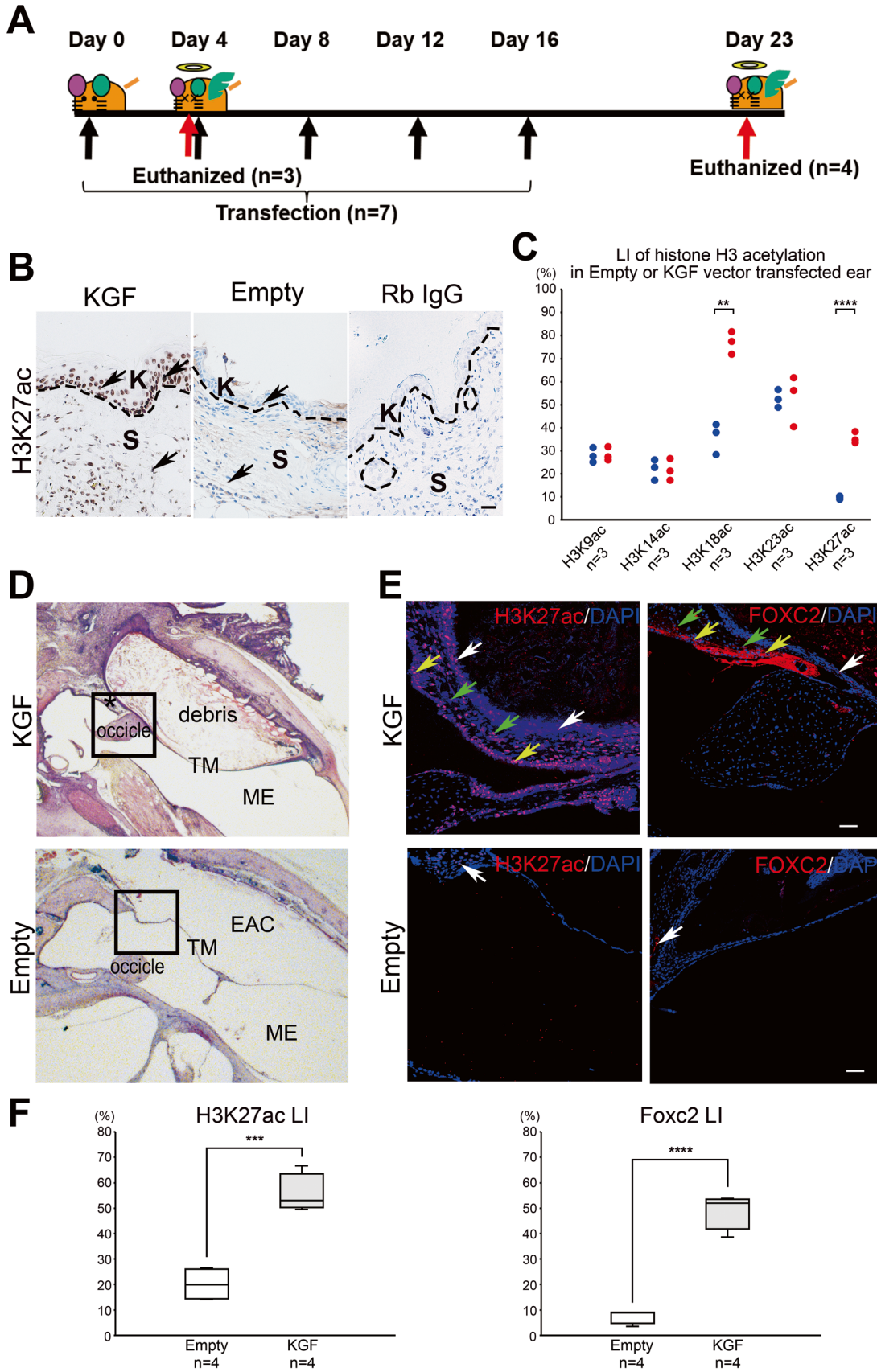
◄**Fig. 4** Keratinocyte growth factor (KGF) gene transfection induced acetylation of histone H3K27 and FOXC2-expression in the cells of mouse ear tissue. **a** Schematic description of the method for electroporated transfection of KGF-expression vector in mouse ear. As a control vector alone transfection was done in the other mouse ears. The animals were euthanized using an intraperitoneal injection of 200 mg/kg pentobarbital and their ear tissue was removed 4 and 23 days after vector transfection. **b** Immunohistochemical detection of H3K27ac in sections of KGF gene-transfected ear skin tissue (KGF; day 4) and vector alone-transfected ear skin tissue (Empty; day 4). H3K27ac-positive cells (arrows) were detected in the epithelium and subepithelial region. No staining was observed with normal rabbit IgG (Rb IgG) instead of first antibody. Dashed lines indicate the basement membrane. K indicates keratinizing squamous epithelium. S indicates the subepithelial region. Scale bar, 20 μm. **c** Dots plot showing labeling index (LI) of acetylated histone H3 at lysine 9, 14, 18, 23, and 27 positive cells in vector alone-transfected ears (day 4, $n = 3$ for each) (Empty, blue dots) and the KGF gene-transfected ears (day 4, $n = 3$ for each) (KGF, red dots). One-way ANOVA with an unpaired t test were used to compare each LI of Empty versus KGF; H3K18ac LI: $F(1, 4) = 72.23$, **, $p < 0.01$; H3K27ac LI: $F(1, 4) = 293.74$, ****, $p < 0.0001$. **d** Hematoxylin and eosin staining in the sections of KGF gene-transfected ears (KGF; day 23) and vector alone-transfected ears (Empty; day 23). KGF gene-transfected ears showed cholesteatoma formation (asterisk) with debris. EAC: ear auditory canal, TM: tympanic membrane, ME: middle ear. **e** Immunofluorescence detection of H3K27ac (left columns) and FOXC2 (right columns) in the sections of Empty and KGF (boxed areas in D). In the region of cholesteatoma many H3K27ac-positive (red) and FOXC2-positive cells (red) were shown in epithelial layer (white arrows), intermediate layer (green arrows) and mucosal layer (yellow arrows). A few H3K27ac-positive (red) and FOXC2-positive cells (red) were shown in TM of Empty. Arrows: positive cells. Scale bars, 50 μm. Nuclei stained with DAPI (4′,6′-diamidino-2-phenylindole) (blue). **f** Box plot showing the H3K27ac LI or FOXC2 LI of in vector alone-transfected ears (Empty, $n = 4$ for each) (white boxes) and KGF gene-transfected ears (KGF, $n = 4$ for each) (gray boxes). One-way ANOVA with an unpaired t test were used to compare Empty versus KGF; H3K27ac LI: $F(1, 6) = 50.64$, ***, $p < 0.001$; FOXC2 LI: $F(1, 6) = 142.34$, ****, $p < 0.0001$

associated with proliferation in the oral squamous cell carcinoma cell line analysis. Initially, we hypothesized that the expression of FOXC2 increased the proliferative activity of epithelial cells in cholesteatoma and analyzed the correlation between the proliferative activity of epithelial cells and FOXC2 LI in cholesteatoma tissues immunohistochemically by using anti-proliferating cell nuclear antigen (PCNA) antibody. Against our expectations, a significant correlation between FOXC2 LI and PCNA LI was not observed (data not shown). FOXC2 also has been shown to induce epithelial mesenchymal transition (EMT) and to serve as a link between EMT and stem cell properties in breast cancer (Mani et al. 2007; Hollier et al. 2013). One of these studies indicated FOXC2 could induce EMT and promote invasion and metastasis by decreasing E-cadherin expression but increasing Snail expression (Cui et al. 2015). Indeed, we indicated partial-EMT was observed during growth of cholesteatoma tissues in our recent study (Takahashi et al 2019), which supports the results of this study.

KGF Enhanced H3K27ac and FOXC2 Expression in Mouse Ear Skin Tissue and KGF-Inducing Cholesteatoma In vivo

In a previous study, we indicated that KGF enhanced epithelial cell proliferative activity and correlated it to the recurrence of human middle ear cholesteatoma (Yamamoto-Fukuda et al. 2003). In addition, we reported that the repetitive electroporatic transfection of the KGF-gene expression vector induced middle ear cholesteatoma formation in vivo (Yamamoto-Fukuda et al. 2015). Based upon these observations, we analyzed the effects of KGF against the acetylation of histone of epithelial and subepithelial cells in our
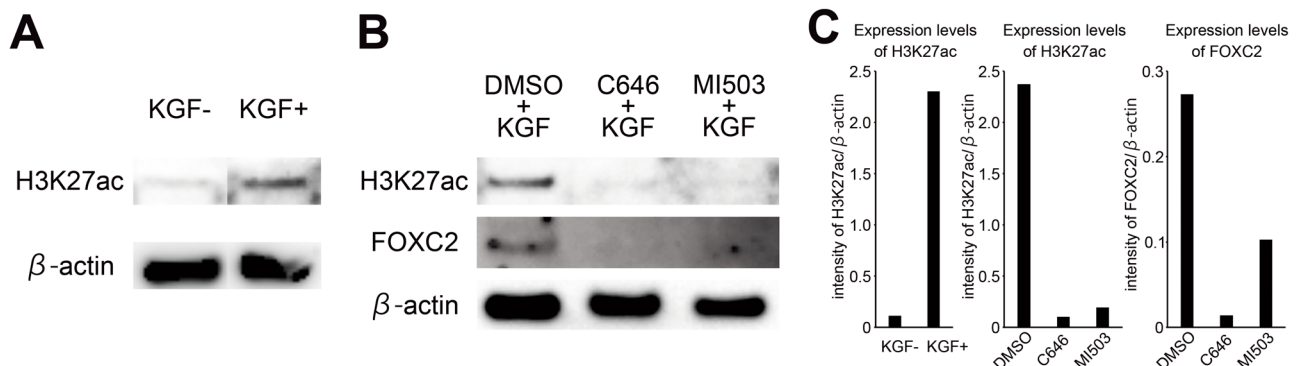
Fig. 5 The expression of FOXC2 under the acetylation of H3K27 induced by KGF was inhibited by the H3K27ac inhibitor (C646) and the menin-MLL inhibitor (MI503). **a** The acetylation of H3K27 was induced by the administration of KGF protein. Western blot analysis of H3K27ac and β-actin in the cells treated with PBS (left lane) or treated with KGF (right lane) (top lane, reacted with anti-H3K27ac antibody; bottom lane, reacted with anti β-actin antibody). **b** Western blot analysis of H3K27ac, FOXC2, and β-actin in the cells of control (left lane), C646 with KGF (middle lane), or MI503 with KGF (right lane) (top lane, reacted with anti-H3K27ac antibody; middle lane, reacted with anti-FOXC2 antibody; bottom lane, reacted with anti-β-actin antibody). **c** Bar graphs showing the expression level of H3K27ac or FOXC2 protein of each group. The signal strength was determined using the intensity of the band divided by the β-actin band intensity. β-Actin was used as a loading control

A

Day 0 Day 1 Day 2 Day 3 Day 4

n=12

→ Transfection   → MI503   → Euthanized

B

KGF+PBS   KGF+MI503 50 µM   KGF+MI503 500 µM

C

Epitherial thickness

(µm)

D

KGF+PBS   KGF+MI503 50 µM   KGF+MI503 500 µM

H3K27ac

Foxc2

E

H3K27ac LI
after topical administration

Foxc2 LI
after topical administration
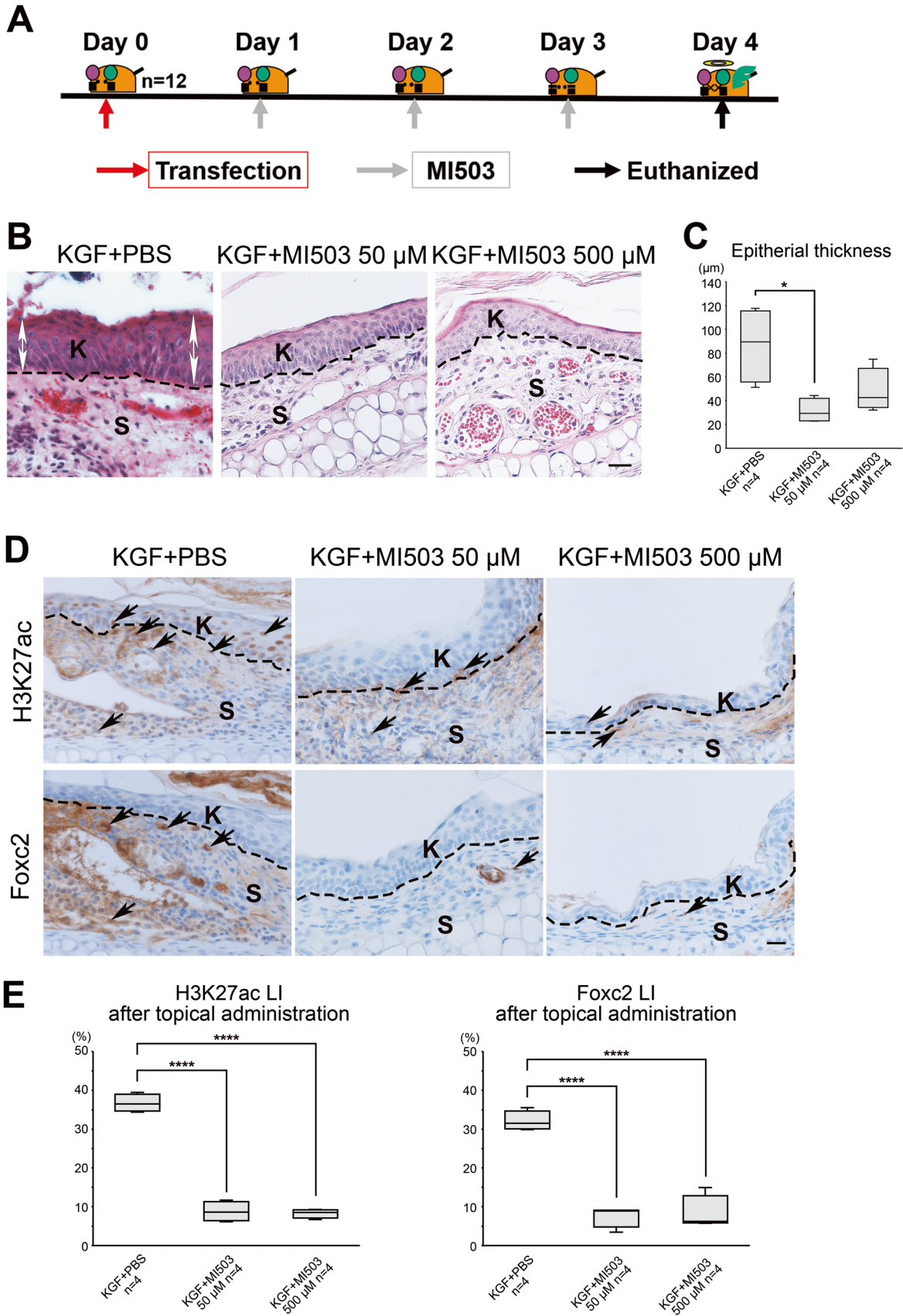
◀ **Fig. 6** Increased expression of FOXC2 under the over-expression of KGF was inhibited by the menin-MLL inhibitor (MI503), an inhibitor for H3K27ac. **a** Schematic description of the method for administration of MI503 in vivo in KGF-transfected mouse ear. The menin-MLL inhibitor (500 μM or 50 μM MI503) or 2% DMSO in PBS (PBS) was administered via eardrops each day every 24 h from the next day of vector transfection to the day before euthanization. The animals were euthanized using an intraperitoneal injection of 200 mg/kg pentobarbital and their ear tissue was removed. **b** Morphological changes in the mouse ear tissues after MI503 administration with KGF gene transfection. H&E staining of ear tissues of KGF + PBS, KGF + MI503 50 μM, and KGF + MI503 500 μM. Double-headed arrows indicate thickened epithelium. Dashed lines indicate the basement membrane. K indicates keratinizing squamous epithelium. S indicates the subepithelial region. Scale bar, 20 μm. **c** Box plot showing the average of the epithelial thickness in the sections of KGF + PBS (86.89 ± 31.7 μm), KGF + MI503 50 μM (31.46 ± 10.1 μm) and KGF + MI503 (47.91 ± 18.6 μm) ($n = 4$ for each) (*$p < 0.05$ as determined by a one-way ANOVA $F(2, 9) = 6.69$ with a Tukey's post hoc test). **d** Immunohistochemical detection of H3K27ac (upper columns) and FOXC2 (lower columns) in the sections of KGF + PBS, KGF + MI503 50 μM, and KGF + MI503. H3K27ac-positive cells (arrows) were detected in the epithelium and subepithelial region of KGF + PBS. MI503 administration was reduced the acetylation of H3K27 in the cells of epithelium and subepithelial region (KGF + MI503 50 μM and KGF + MI503 500 μM). FOXC2-positive cells (arrows) were detected in the subepithelial region of KGF + PBS. MI503 administration was reduced the expression of FOXC2 (KGF + MI503 50 μM and KGF + MI503 500 μM). Arrows indicate positive cells. Dashed lines indicate the basement membrane. K indicates keratinizing squamous epithelium. S indicates the subepithelial region. Scale bar, 20 μm. **e** Box plot showing the H3K27ac LI or FOXC2 LI of KGF + PBS, KGF + MI503 50 μM and KGF + MI503 500 μM ($n = 4$ for each) (one-way ANOVA with a Tukey's post hoc test; H3K27ac LI: $F(2, 9) = 253.54$, ***, $p < 0.0001$; FOXC2 LI: $F(2, 9) = 69.88$, ****, $p < 0.0001$)

in vivo model. The transfection of the hKGF-expression vector by electroporation increased the H3K27ac level in the thick keratinized epithelial and subepithelial regions of the ear skin tissue and also in the cholesteatoma induced by the hKGF-expression vector (Fig. 4). The localization of H3K27ac-positive cells was the same as that of human cholesteatoma (Fig. 1, Fig. 4). However, FOXC2 expression was detected both in the cells of the subepithelial region and in the mucosal layers, but scarcely detected in the cells of the keratinized epithelial layer in the mouse model (Fig. 4).

In the previous study, we showed that p63-positive stem/progenitor cells increased in the thickened epithelium after KGF transfection in vivo (Yamamoto-Fukuda et al. 2018). The p63 gene, a homologue of the tumor suppressor p53, is highly expressed in the basal or progenitor layers of many epithelial tissues and it is likely that p63 preserves the self-renewal capacity of progenitor cells (Yang et al. 1998). Therefore, we concluded that p63 might be critical for maintaining the progenitor cell populations necessary to sustain epithelial hyper-proliferation and morphogenesis of middle ear cholesteatoma (Yamamoto-Fukuda et al. 2018). Previously, Kouwenhoven and colleagues (2015) showed that the activity of p63 binding sites, as defined by the co-localization of histone modification mark H3K27ac signals, correlates with the expression of nearby genes, which are associated with distinct skin disease phenotypes. They also concluded that the dynamics of gene expression correlated with the activity of p63-bound enhancers plays a role in keratinocyte differentiation rather than that of p63 binding itself (Kouwenhoven et al. 2015). Taken together with our previous results and these observations, it is possible that the genes activated by the p63-bound enhancers, which are associated with the epithelial cells of cholesteatoma, might be masked by the results of H3K27ac ChIP-seq analysis. In this regard, we should do a combined analysis of p63 ChIP-seq and H3K27ac ChIP-seq to detect the genes that are in active p63 binding sites with the H3K27ac mark as target genes associated with the pathogenesis of epithelial cells in cholesteatoma in the future.

FOXC2-expression was detected in the mucosal layer of the TM in KGF-induced cholesteatoma in vivo. There is another possibility that the effects of KGF on FOXC2-expressed mucosal epithelia in the TM may strongly accelerate cellular turnover and differentiate into the keratinizing epithelia that consists of cholesteatoma. It has been documented that FOXC2 directly induces the transcription of CXCR4 by activating its promoters and is associated with angiogenesis (Li et al. 2011). They showed that FOXC2-positive endothelial progenitor cells increased migration and adhesion capacity, and also indicated that FOXC2 overexpression enhances the homing capacity of endothelial progenitor cells and improved reendothelialization (Li et al. 2011). This supports our hypothesis. There is another

TABLE 3

Epithelial thickness and LI of H3K27ac- and FOXC2-positive cells of the ear epithelium treated with MI503 or 2% DMSO in PBS (vehicle) after KGF gene transfection

	Epithelial thickness	H3K27ac	FOXC2
KGF + MI503 50 μM ($n = 4$)	31.46 ± 10.1	8.74 ± 2.5	7.56 ± 2.8
KGF + MI503 500 μM ($n = 4$)	47.91 ± 18.6	8.25 ± 1.2	8.29 ± 4.4
KGF + 1% DMSO/PBS ($n = 4$)	86.89 ± 31.7*	36.73 ± 2.2****	32.11 ± 2.5****

****$p < 0.0001$, *$p < 0.05$; **$p < 0.0001$

study that showed that high expression of *FOXC2*-mRNA was detected in keratinocytes in a primary culture harvested from human TM tissues as compared with normal human skin keratinocytes by real-time reverse transcription polymerase chain reaction (Sagiv et al. 2019). By contrast, in our study FOXC2 was not detected in the keratinizing epithelia of the TM without KGF stimulation (Fig. 4). One possibility is that growth factors contained in the culture media, keratinocyte serum-free medium and progenitor cell medium in a 1:1 ratio, might accelerate *FOXC2*-mRNA expressed in the primary culture keratinocyte (Sagiv et al. 2019). Indeed, the recent study indicated that insulin, which was in this culture media for keratinocyte, promoted the expression of *FOXC2*-mRNA in prostate cancer cells (Sarkar et al. 2019).

Treatment with MI503, a Menin-MLL Inhibitor, Suppressed H3K27ac and FOXC2 Expression, Resulting in the Suppression of Hyperproliferation of the Epithelium

To determine whether KGF induces an acetylation of H3K27 in middle ear epithelial cells, we first did an in vitro assay. The primary middle ear epithelial cells were treated with or without rhKGF protein (10 ng/ml) overnight and the expression level of H3K27ac was analyzed in the whole cell lysates by western blot analysis. According to the results, a high level of H3K27ac-expression was detected in the rhKGF-treated cells (Fig. 5a). During development, FGF signaling increases levels of H3K27ac by recruiting p300 HAT (Peluso et al. 2017). KGF is a member of the FGF family and plays a role in the differentiation of lung epithelial cells and oral epithelial cells during development (Finch et al. 1995; Otsuka-Tanaka et al. 2013). These facts supported our results that KGF signaling induces H3K27ac, which is required to activate some genes associated with the pathogenesis of cholesteatoma. Next, we analyzed the upstream of FOXC2 expression under KGF signaling by using H3K27ac inhibitor (C646) in vitro. C646 is a p300 HAT inhibitor and it directly inhibits the acetylation of H3K27 (Li et al. 2019). According to the results, FOXC2 expression was suppressed in the middle ear cells treated with H3K27ac inhibitor (Fig. 5b). In other words, the induction of H3K27ac under KGF signaling might induce the expression of FOXC2 in middle ear cells. A menin-MLL1 inhibitor, MI503, is known as an inhibitor of trimethylation of H3K4 (Malik et al. 2015). Interestingly, recent studies demonstrated that H3K4me3 and H3K27ac are contained looped enhancers bounded by menin and MLL1 and MLL2; in other words, menin-H3K4me3-dependent gene regulation marked by menin-bound TSS connected to the canonical enhancer

histone mark H3K27ac (Dreijerink et al. 2017). To analyze the effects of menin-MLL inhibitor (MI503) as a H3K27ac inhibitor, we also treated the middle ear cells with MI503 before KGF administration. According to the results, MI503 inhibited the acetylation of H3K27 and reduced the expression of FOXC2 in the middle ear epithelial cells (Fig. 5b).

To confirm the induction of H3K27ac under KGF signaling induced the expression of FOXC2 in mouse cholesteatoma model, we performed KGF-gene transfection with menin-MLL inhibitor (MI503) or 2% DMSO in PBS in a mouse ear in vivo (Fig. 6). As expected, the number of H3K27ac-positive cells in the MI503-treated ear had decreased and thickening of the epithelium was reduced (Fig. 6). The menin-MLL complex can directly bind on histone-marked promoters and coding regions of its target genes and induce leukemia and prostate cancer (Shi et al. 2012; Malik et al. 2015). Recently, menin-MLL inhibitor has attracted attention as a therapeutic drug and several menin-MLL inhibitors, including KO-539 and SNDX-5613, are now in clinical trials for leukemia patients. In addition, Kempinska and colleagues (2018) demonstrated that the menin-MLL inhibitor MI-503 showed antitumor activity in the in vitro and in vivo models of hepatic cell carcinoma.

In our study, FOXC2 expression was consistently upregulated and detected in the subepithelial region in the mouse ear and thickened epithelium was induced at day 4 after KGF gene transfection (Fig. 6). Furthermore, by using an inhibitor of H3K27ac, MI503 in vivo, the number of FOXC2-positive cells in the subepithelial region was shown to have decreased (Fig. 6). Many reports indicate that FOXC2 loss-of-function causes pre- and perinatal death in association with skeletal, genitourinary tract and cardiovascular defects (Iida et al. 1997; Winnier et al. 1999; Kume et al. 2001; Kanzaki-Kato et al. 2005; Seo and Kume 2006). However, the expression of FOXC2 decreases after the developmental stage and is expressed in adipose tissues under the conditions of obesity (Nishida et al. 2011; Zhu et al. 2013; Jiang et al. 2012; Imayama et al. 2015; Cederberg et al. 2001) and carcinogenesis in adults (Li et al. 2013). Since FOXC2 is abnormally expressed in cholesteatoma, it is considered to be a good therapeutic target for promoting the suppression of FOXC2 expression with MI503. In fact, many recent studies have analyzed FOXC2 as a therapeutic target for disease (Pan and Xie 2020; Bi et al. 2020; Chen et al. 2020), the same as with our study.

In conclusion, KGF may accelerate the acetylation of H3K27 and the induction of FOXC2 expression of cells in the TM, resulting in epithelial hyperplasia and stratification with debris, as in cholesteatoma formation. Controlling the modification of histone acetylation is a potentially suitable therapeutic target for the conservative treatment of cholesteatoma in the future.

ACKNOWLEDGEMENTS

Availability of Data and Material The datasets produced and/or analyzed during the current study are available from the corresponding author upon reasonable request.

Code Availability The study uses data obtained from the UCSC genome browser http://genome.ucsc.edu/index.html.

DECLARATIONS

Ethics Approval All the experimental procedures were performed in accordance with the Nagasaki University with the approval of the Institutional Animal Care and Use Committee (Nos. 1209241015-2 and 1404011269), the Guidelines for Animal Experimentation of Jikei University with approval guidelines (No. 2015-139C4), the Human Ethics Review Committee of Jikei University School of Medicine (approval number is 27-344 8229).

Consent for Publication This study protocol was approved by the Human Ethics Review Committee of Jikei University School of Medicine, and signed informed consent was obtained from all the patients or their guardians for this study (approval number is 27-344 8229).

Conflict of Interest The authors declare no competing interests.

REFERENCES

Akiyama N, Yamamoto-Fukuda T, Takahashi H (2014) Influence of continuous negative pressure in the rat middle ear. Laryngoscope 124:2404–2410. https://doi.org/10.1002/lary.24767

Bi Y, Guo S, Xu X, Kong P, Cui H, Yan T, Ma Y, Cheng Y, Chen Y, Liu X, Zhang L, Cheng C, Xu E, Qian Y, Yang J, Song B, Li H, Wang F, Hu X, Liu X, Niu X, Zhai Y, Liu J, Li Y, Cheng X, Cui Y (2020) Decreased ZNF750 promotes angiogenesis in a paracrine manner via activating DANCR/miR-4707-3p/FOXC2 axis in esophageal squamous cell carcinoma. Cell Death Dis 11:296. https://doi.org/10.1038/s41419-020-2492-2

Borkin D, He S, Miao H, Kempinska K, Pollock J, Chase J, Purohit T, Malik B, Zhao T, Wang J, Wen B, Zong H, Jones M, Danet-Desnoyers G, Guzman ML, Talpaz M, Bixby DL, Sun D, Hess JL, Muntean AG, Maillard I, Cierpicki T, Grembecka J (2015) Pharmacologic inhibition of the menin-MLL interaction blocks progression of MLL leukemia in vivo. Cancer Cell 27:589–602. https://doi.org/10.1016/j.ccell.2015.02.016

Bowers EM, Yan G, Mukherjee C, Orry A, Wang L, Holbert MA, Crump NT, Hazzalin CA, Liszczak G, Yuan H, Larocca C, Saldanha SA, Abagyan R, Sun Y, Meyers DJ, Marmorstein R, Mahadevan LC, Alani RM, Cole PA (2010) Virtual ligand screening of the p300/CBP histone acetyl transferase: identification of a selective small molecule inhibitor. Chem Biol 17:471–482. https://doi.org/10.1016/j.chembiol.2010.03.006

Braun S, Krampert M, Bodó E, Kümin A, Born-Berclaz C, Paus R, Werner S (2006) Keratinocyte growth factor protects epidermis and hair follicles from cell death induced by UV irradiation, chemotherapeutic or cytotoxic agents. J Cell Sci 119:4841–4849. https://doi.org/10.1242/jcs.03259

Calo E, Wysocka J (2013) Modification of enhancer chromatin: what, how, and why? Mol Cell 49:825–837. https://doi.org/10.1016/j.molcel.2013.01.038

Cederberg A, Grønning LM, Ahrén B, Taskén K, Carlsson P, Enerbäck S (2001) FOXC2 is a winged helix gene that counteracts obesity, hypertriglyceridemia, andiet-induced insulin resistance. Cell 106:563–573. https://doi.org/10.1016/s0092-8674(01)00474-3

Chapuy B, McKeown MR, Lin CY, Monti S, Roemer MGM, Qi J, Rahl PB, Sun HH, Yeda KT, Doench JG, Reichert E, Kung AL, Rodig SJ, Young RA, Shipp MA, Bradner JE (2013) Discovery and characterization of super-enhancer-associated dependencies in diffuse large b cell lymphoma. Cancer Cell 24(6):777-90. https://doi.org/10.1016/j.ccr.2013.11.003

Chen Y, Deng G, Fu Y, Han Y, Guo C, Yin L, Cai C, Shen H, Wu S, Zeng S (2020) FOXC2 promotes oxaliplatin resistance by inducing epithelial-mesenchymal transition via MAPK/ERK signaling in colorectal cancer. Onco Targets Ther 13:1625–1635. https://doi.org/10.2147/OTT.S241367

Chi Z, Wang Z, Liang Q, Zhu Y, du Q, (2015) Induction of cytokine production in cholesteatoma keratinocytes by extracellular high-mobility group box chromosomal protein 1 combined with DNA released by apoptotic cholesteatoma keratinocytes. Mol Cell Biochem 400:189–200. https://doi.org/10.1007/s11010-014-2275-0

Creyghton MP, Cheng AW, Welstead GG, Kooistra T, Carey BW, Steine EJ, Hanna J, Lodato MA, Frampton GM, Sharp PA, Boyer LA, Young RA, Jaenisch R (2010) Histone H3K27ac separates active from poised enhancers and predicts developmental state. Proc Natl Acad Sci U S A 107:21931–21936. https://doi.org/10.1073/pnas.1016071107

Crish JF, Eckert RL (2008) Synergistic activation of human involucrin gene expression by Fra-1 and p300–evidence for the presence of a multiprotein complex. J Invest Dermatol 128:530–541. https://doi.org/10.1038/sj.jid.5701049

Cui YM, Jiao HL, Ye YP, Chen CM, Wang JX, Tang N, Li TT, Lin J, Qi L, Wu P, Wang SY, He MR, Liang L, Bian XW, Liao WT, Ding YQ (2015) FOXC2 promotes colorectal cancer metastasis by directly targeting MET. Oncogene 34:4379–4390. https://doi.org/10.1038/onc.2014.368

Dawson MA, Kouzarides T (2012) Cancer epigenetics: from mechanism to therapy. Cell 150:12–27. https://doi.org/10.1016/j.cell.2012.06.013

Djebali S, Davis CA, Merkel A et al (2012) Landscape of transcription in human cells. Nature 489:101–108. https://doi.org/10.1038/nature11233

Dreijerink KMA, Groner AC, Vos ESM, Font-Tello A, Gu L, Chi D, Reyes J, Cook J, Lim E, Lin CY, de Laat W, Rao PK, Long HW, Brown M (2017) Enhancer-mediated oncogenic function of the menin tumor suppressor in breast cancer. Cell Rep 18:2359–2372. https://doi.org/10.1016/j.celrep.2017.02.025

Ernst J, Kheradpour P, Mikkelsen TS, Shoresh N, Ward LD, Epstein CB, Zhang X, Wang L, Issner R, Coyne M, Ku M, Durham T, Kellis M, Bernstein BE (2011) Mapping and analysis of chromatin state dynamics in nine human cell types. Nature 473:43–49. https://doi.org/10.1038/nature09906

Ficz G, Hore TA, Santos F, Lee HJ, Dean W, Arand J, Krueger F, Oxley D, Paul YL, Walter J, Cook SJ, Andrews S, Branco MR, Reik W (2013) FGF signaling inhibition in ESCs drives rapid genome-wide demethylation to the epigenetic ground state of pluripotency. Cell Stem Cell 13:351–359. https://doi.org/10.1016/j.stem.2013.06.004

Finch PW, Cunha GR, Rubin JS, Wong J, Ron D (1995) Pattern of keratinocyte growth factor and keratinocyte growth factor receptor expression during mouse fetal development suggests a role in mediating morphogenetic mesenchymal-epithelial interactions. Dev Dyn 203:223–240. https://doi.org/10.1002/aja.1002030210

Heintzman ND, Stuart RK, Hon G, Fu Y, Ching CW, Hawkins RD, Barrera LO, Van Calcar S, Qu C, Ching KA, Wang W, Weng Z, Green RD, Crawford GE, Ren B (2007) Distinct and predictive chromatin signatures of transcriptional promoters and enhancers in the human genome. Nat Genet 39:311–318. https://doi.org/10.1038/ng1966

Hnisz D, Abraham BJ, Lee TI, Lau A, Saint-Andre V, Sigova AA, Hoke HA, Young RA (2013) Super-enhancers in the control of cell identity and disease. Cell 155:934–947. https://doi.org/10.1016/j.cell.2013.09.053

Hollier BG, Tinnirello AA, Werden SJ, Evans KW, Taube JH, Sarkar TR, Sphyris N, Shariati M, Kumar SV, Battula VL, Herschkowitz JI, Guerra R, Chang JT, Miura N, Rosen JM, Mani SA (2013) FOXC2 expression links epithelial-mesenchymal transition and stem cell properties in breast cancer. Cancer Res 73:1981–1992. https://doi.org/10.1158/0008-5472.CAN-12-2962

Iida K, Koseki H, Kakinuma H, Kato N, Mizutani-Koseki Y, Ohuchi H, Yoshioka H, Noji S, Kawamura K, Kataoka Y, Ueno F, Taniguchi M, Yoshida N, Sugiyama T, Miura N (1997) Essential roles of the winged helix transcription factor MFH-1 in aortic arch patterning and skeletogenesis. Development 124:4627–4638

Imayama N, Yamada S, Yanamoto S, Naruse T, Matsushita Y, Takahashi H, Seki S, Fujita S, Ikeda T, Umeda M (2015) FOXC2 expression is associated with tumor proliferation and invasion potential in oral tongue squamous cell carcinoma. Pathol Oncol Res 21:783–791. https://doi.org/10.1007/s12253-014-9891-6

Ito K, Ito M, Elliott WM, Cosio B, Caramori G et al (2005) Decreased histone deacetylase activity in chronic obstructive pulmonary disease. N Engl J Med 352:1967–1976. https://doi.org/10.1056/NEJMoa041892

Jiang W, Pang XG, Wang Q, Shen YX, Chen XK, Xi JJ (2012) Prognostic role of Twist, Slug, and Foxc2 expression in stage I non-small-cell lung cancer after curative resection. Clin Lung Cancer 13:280–287. https://doi.org/10.1016/j.cllc.2011.11.005

Kanzaki-Kato N, Tamakoshi T, Fu Y, Chandra A, Itakura T, Uezato T, Tanaka T, Clouthier DE, Sugiyama T, Yanagisawa M, Miura N (2005) Roles of forkhead transcription factor Foxc2 (MFH-1) and endothelin receptor A in cardiovascular morphogenesis. Cardiovasc Res 65:711–718. https://doi.org/10.1016/j.cardiores.2004.10.017

Kempinska K, Malik B, Borkin D, Klossowski S, Shukla S, Miao H, Wang J, Cierpicki T, Grembecka J (2018) Pharmacologic Inhibition of the Menin-MLL interaction leads to transcriptional repression of PEG10 and blocks hepatocellular carcinoma. Mol Cancer Ther 17:26–38. https://doi.org/10.1158/1535-7163.MCT-17-0580

Kouwenhoven EN, Oti M, Niehues H, van Heeringen SJ, Schalkwijk J, Stunnenberg HG, van Bokhoven H, Zhou H (2015) Transcription factor p63 bookmarks and regulates dynamic enhancers during epidermal differentiation. EMBO Rep 16:863–878. https://doi.org/10.15252/embr.201439941

Kume T, Jiang H, Topczewska JM, Hogan BL (2001) The murine winged helix transcription factors, Foxc1 and Foxc2, are both required for cardiovascular development and somitogenesis. Genes Dev 15:2470–2482. https://doi.org/10.1101/gad.907301

Kuo CL (2015) Etiopathogenesis of acquired cholesteatoma: prominent theories and recent advances in biomolecular research. Laryngoscope 125:234–240. https://doi.org/10.1002/lary.24890

Lee JS, See RH, Deng T, Shi Y (1996) Adenovirus E1A downregulates cJun- and JunB-mediated transcription by targeting their coactivator p300. Mol Cell Biol 16:4312–4326. https://doi.org/10.1128/mcb.16.8.4312

Lee K, Hsiung CC, Huang P, Raj A, Blobel GA (2015) Dynamic enhancer-gene body contacts during transcription elongation. Genes Dev 29:1992–1997. https://doi.org/10.1101/gad.255265.114

Li D, Yan D, Liu W, Li M, Yu J, Li Y, Qu Z, Ruan Q (2011) Foxc2 overexpression enhances benefit of endothelial progenitor cells for inhibiting neointimal formation by promoting CXCR4-dependent homing. J Vasc Surg 53:1668–1678. https://doi.org/10.1016/j.jvs.2011.01.044

Li QL, Wang DY, Ju LG, Yao J, Gao C, Lei PJ, Li LY, Zhao XL, Wu M (2019) The hyper-activation of transcriptional enhancers in breast cancer. Clin Epigenetics 11:48. https://doi.org/10.1186/s13148-019-0645-x

Li W, Fu X, Liu R, Wu C, Bai J, Xu Y, Zhao Y, Xu Y (2013) FOXC2 often overexpressed in glioblastoma enhances proliferation and invasion in glioblastoma cells. Oncol Res 21:111–120. https://doi.org/10.3727/096504013X13814233062171

Lovén J, Hoke HA, Lin CY, Lau A, Orlando DA, Vakoc CR, Bradner JE, Lee TI, Young RA (2013) Selective inhibition of tumor oncogenes by disruption of super-enhancers. Cell 153:320–334. https://doi.org/10.1016/j.cell.2013.03.036

Malik R, Khan AP, Asangani IA, Cieślik M, Prensner JR, Wang X, Iyer MK, Jiang X, Borkin D, Escara-Wilke J, Stender R, Wu YM, Niknafs YS, Jing X, Qiao Y, Palanisamy N, Kunju LP, Krishnamurthy PM, Yocum AK, Mellacheruvu D, Nesvizhskii AI, Cao X, Dhanasekaran SM, Feng FY, Grembecka J, Cierpicki T, Chinnaiyan AM (2015) Targeting the MLL complex in castration-resistant prostate cancer. Nat Med 21:344–352. https://doi.org/10.1038/nm.3830.

Mani SA, Yang J, Brooks M, Schwaninger G, Zhou A, Miura N, Kutok JL, Hartwell K, Richardson AL, Weinberg RA (2007) Mesenchyme Forkhead 1 (FOXC2) plays a key role in metastasis and is associated with aggressive basal-like breast cancers. Proc Natl Acad Sci USA 104:10069–10074. https://doi.org/10.1073/pnas.0703900104

Matsumoto K, Nagayasu T, Hishikawa Y, Tagawa T, Yamayoshi T, Abo T, Tobinaga S, Furukawa K, Koji T (2009) Keratinocyte growth factor accelerates compensatory growth in the remaining lung after trilobectomy in rats. J Thorac Cardiovasc Surg 137:1499–1507. https://doi.org/10.1016/j.jtcvs.2008.11.037

Milne TA, Hughes CM, Lloyd R, Yang Z, Rozenblatt-Rosen O, Dou Y, Schnepp RW, Krankel C, Livolsi VA, Gibbs D, Hua X, Roeder RG, Meyerson M, Hess JL (2005) Menin and MLL cooperatively regulate expression of cyclin-dependent kinase inhibitors.

Proc Natl Acad Sci U S A 102:749–754. https://doi.org/10.1073/pnas.0408836102

Nishida N, Mimori K, Yokobori T, Sudo T, Tanaka F, Shibata K, Ishii H, Doki Y, Mori M (2011) FOXC2 is a novel prognostic factor in human esophageal squamous cell carcinoma. Ann Surg Oncol 18:535–542. https://doi.org/10.1245/s10434-010-1274-y

Otsuka-Tanaka Y, Oommen S, Kawasaki M, Kawasaki K, Imam N, Jalani-Ghazani F, Hindges R, Sharpe PT, Ohazama A (2013) Oral lining mucosa development depends on mesenchymal microRNAs. J Dent Res 92:229–234. https://doi.org/10.1177/0022034512470830

Pan K, Xie Y (2020) LncRNA FOXC2-AS1 enhances FOXC2 mRNA stability to promote colorectal cancer progression via activation of Ca (2+)-FAK signal pathway. Cell Death Dis 11:434. https://doi.org/10.1038/s41419-020-2633-7

Peluso S, Douglas A, Hill A, De Angelis C, Moore BL, Grimes G, Petrovich G, Essafi A, Hill RE (2017) Fibroblast growth factors (FGFs) prime the limb specific Shh enhancer for chromatin changes that balance histone acetylation mediated by E26 transformation-specific (ETS) factors. Elife ;6:e28590. https://doi.org/10.7554/eLife.28590.

Raisner R, Kharbanda S, Jin L, Jeng E, Chan E, Merchant M, Haverty PM, Bainer R, Cheung T, Arnott D, Flynn EM, Romero FA, Magnuson S, Gascoigne KE (2018) Enhancer activity requires CBP/P300 bromodomain-dependent histone H3K27 acetylation. Cell Rep 24:1722–1729. https://doi.org/10.1016/j.celrep.2018.07.041

Sagiv D, Harari-Steinberg O, Wolf M, Dekel B, Omer D (2019) The feasibility to isolate and expand tympanic membrane squamous epithelium stem cells from scarred perforation margins. Otol Neurotol 40:e1030–e1036. https://doi.org/10.1097/MAO.0000000000002367

Schneider CA, Rasband WS, Eliceiri KW (2012) NIH Image to ImageJ: 25 years of image analysis. Nat Methods 9:671–675. https://doi.org/10.1038/nmeth.2089

Schuettengruber B, Chourrout D, Vervoort M, Leblanc B, Cavalli G (2007) Genome regulation by polycomb and trithorax proteins. Cell 128:735–745. https://doi.org/10.1016/j.cell.2007.02.009

Seo S, Kume T (2006) Forkhead transcription factors, Foxc1 and Foxc2, are required for the morphogenesis of the cardiac outflow tract. Dev Biol 296:421–436. https://doi.org/10.1016/j.ydbio.2006.06.012

Sarkar PL, Lee W, Williams ED, Lubik AA, Stylianou N, Shokoohmand A, Lehman ML, Hollier BG, Gunter JH, Nelson CC (2019) Insulin enhances migration and invasion in prostate cancer cells by up-regulation of FOXC2. Front Endocrinol (Lausanne) 10:481. https://doi.org/10.3389/fendo.2019.00481

Shi A, Murai MJ, He S, Lund G, Hartley T, Purohit T, Reddy G, Chruszcz M, Grembecka J, Cierpicki T (2012) Structural insights into inhibition of the bivalent menin-MLL interaction by small molecules in leukemia. Blood 120:4461–4469. https://doi.org/10.1182/blood-2012-05-429274

Song N, Liu J, An S, Nishino T, Hishikawa Y, Koji T (2011) Immunohistochemical analysis of histone H3 modifications in germ cells during mouse spermatogenesis. Acta Histochem Cytochem 44:183–190. https://doi.org/10.1267/ahc.11027

Sudhoff H, Tos M (2000) Pathogenesis of attic cholesteatoma: clinical and immunohistochemical support for combination of retraction theory and proliferation theory. Am J Otol 21:786–792

Takahashi M, Yamamoto-Fukuda T, Akiyama N, Motegi M, Yamamoto K, Tanaka Y, Yamamoto Y, Kojima H (2019) Partial epithelial-mesenchymal transition was observed under p63 expression in acquired middle ear cholesteatoma and congenital cholesteatoma. Otol Neurotol 40:e803–e811. https://doi.org/10.1097/MAO.0000000000002328

Tambalo M, Anwar M, Ahmed M, Streit A (2020) Enhancer activation by FGF signalling during otic induction. Dev Biol 457:69–82. https://doi.org/10.1016/j.ydbio.2019.09.006

Tanaka Y, Kojima H, Miyazaki H, Koga T, Moriyama H (1999) Roles of cytokines and cell cycle regulating substances in proliferation of cholesteatoma epithelium. Laryngoscope 109:1102–1107. https://doi.org/10.1097/00005537-199907000-00017

Tie F, Banerjee R, Stratton CA, Prasad-Sinha J, Stepanik V, Zlobin A, Diaz MO, Scacheri PC, Harte PJ (2009) CBP-mediated acetylation of histone H3 lysine 27 antagonizes Drosophila Polycomb silencing. Development 136:3131–3141. https://doi.org/10.1242/dev.037127

Vijayakrishnan J, Qian M, Studd JB, Yang W, Kinnersley B, Law PJ, Broderick P, Raetz EA, Allan J, Pui CH, Vora A, Evans WE, Moorman A, Yeoh A, Yang W, Li C, Bartram CR, Mullighan CG, Zimmerman M, Hunger SP, Schrappe M, Relling MV, Stanulla M, Loh ML, Houlston RS, Yang JJ (2019) Identification of four novel associations for B-cell acute lymphoblastic leukaemia risk. Nat Commun 10:5348. https://doi.org/10.1038/s41467-019-13069-6

Wang Z, Zang C, Rosenfeld JA, Schones DE, Barski A, Cuddapah S, Cui K, Roh TY, Peng W, Zhang MQ, Zhao K (2008) Combinatorial patterns of histone acetylations and methylations in the human genome. Nat Genet 40:897–903. https://doi.org/10.1038/ng.154

Whyte WA, Orlando DA, Hnisz D, Abraham BJ, Lin CY, Kagey MH, Rahl PB, Lee TI, Young RA (2013) Master transcription factors and mediator establish super-enhancers at key cell identity genes. Cell 153:307–319. https://doi.org/10.1016/j.cell.2013.03.035

Winnier GE, Kume T, Deng K et al. (1999) Roles for the winged helix transcription factors MF1 and MFH1 in cardiovascular development revealed by nonallelic noncomplementation of null alleles. Dev Biol 213:418–431. https://doi.org/10.1006/dbio.1999.9382

Yamamoto-Fukuda T, Akiyama N, Kojima H (2020) L1CAM-ILK-YAP mechanotransduction drives proliferative activity of epithelial cells in middle ear cholesteatoma. Am J Pathol 190:1667–1679. https://doi.org/10.1016/j.ajpath.2020.04.007

Yamamoto-Fukuda T, Akiyama N, Takahashi M, Kojima H (2018) Keratinocyte growth factor (KGF) modulates epidermal progenitor cell kinetics through activation of p63 in middle ear cholesteatoma. J Assoc Res Otolaryngol 19:223–241. https://doi.org/10.1007/s10162-018-0662-z

Yamamoto-Fukuda T, Akiyama N, Shibata Y, Takahashi H, Ikeda T, Koji T (2015) In vivo over-expression of KGF mimic human middle ear cholesteatoma. Eur Arch Otorhinolaryngol 272:2689–2696. https://doi.org/10.1007/s00405-014-3237-6

Yamamoto-Fukuda T, Akiyama N, Shibata Y, Takahashi H, Ikeda T, Kohno M, Koji T (2014) KGFR as a possible therapeutic target in middle ear cholesteatoma. Acta Otolaryngol 134:1121–1127. https://doi.org/10.3109/00016489.2014.907501

Yamamoto-Fukuda T, Aoki D, Hishikawa Y, Takahashi H, Kobayashi T, Koji T (2003) Possible involvement of keratinocyte growth factor and its receptor in enhanced epithelial-cell proliferation and acquired recurrence of middle-ear cholesteatoma. Lab Invest 83:123–136. https://doi.org/10.1097/01.lab.0000050763.64145.cb

Yamamoto-Fukuda T, Shibata Y, Hishikawa Y, Shin M, Yamaguchi A, Kobayashi T, Koji T (2000) Effects of various decalcification protocols on detection of DNA strand breaks by terminal dUTP nick end labelling. Histochem J 32:697–702. https://doi.org/10.1023/a:1004171517639

Yamamoto-Fukuda T, Akiyama N, Tatsumi N, Okabe M, Kojima H (2021) Menin-MLL inhibitor blocks progression of middle ear cholesteatoma in vivo. Int J Pediatr Otorhinolaryngol 140:110545. https://doi.org/10.1016/j.ijporl.2020.110545

Yang A, Kaghad M, Wang Y, Gillett E, Fleming MD, Dötsch V, Andrews NC, Caput D, McKeon F (1998) p63, a p53 homolog at 3q27-29, encodes multiple products with transactivating, death-inducing, and dominant-negative activities. Mol Cell 2:305–316. https://doi.org/10.1016/s1097-2765(00)80275-0

Zentner GE, Tesar PJ, Scacheri PC (2011) Epigenetic signatures distinguish multiple classes of enhancers with distinct cellular functions. Genome Res 21:1273–1283. https://doi.org/10.1101/gr.122382.111

Zhu JL, Song YX, Wang ZN, Gao P, Wang MX, Dong YL, Xing CZ, Xu HM (2013) The clinical significance of mesenchyme forkhead 1 (FoxC2) in gastric carcinoma. Histopathology 62:1038–1048. https://doi.org/10.1111/his.12132